biomolecules

MDPI

Article

Multi-Omics Analysis of Multiple Glucose-Sensing Receptor Systems in Yeast

Shuang Li [1], Yuanyuan Li [2], Blake R. Rushing [2], Sarah E. Harris [3], Susan L. McRitchie [2], Daniel Dominguez [1], Susan J. Sumner [2,*] and Henrik G. Dohlman [1,*]

[1] Department of Pharmacology, University of North Carolina at Chapel Hill, Chapel Hill, NC 27599, USA; shuang9@email.unc.edu (S.L.); didoming@email.unc.edu (D.D.)
[2] Nutrition Research Institute, Department of Nutrition, School of Public Health, University of North Carolina at Chapel Hill, Kannapolis, NC 28081, USA; yuanyli4@unc.edu (Y.L.); blake_rushing@unc.edu (B.R.R.); susan_mcritchie@unc.edu (S.L.M.)
[3] Department of Biochemistry and Biophysics, University of North Carolina at Chapel Hill, Chapel Hill, NC 27599, USA; harrse@live.unc.edu
* Correspondence: susan_sumner@unc.edu (S.J.S.); hdohlman@med.unc.edu (H.G.D.)

Abstract: The yeast *Saccharomyces cerevisiae* has long been used to produce alcohol from glucose and other sugars. While much is known about glucose metabolism, relatively little is known about the receptors and signaling pathways that indicate glucose availability. Here, we compare the two glucose receptor systems in *S. cerevisiae*. The first is a heterodimer of transporter-like proteins (transceptors), while the second is a seven-transmembrane receptor coupled to a large G protein (Gpa2) that acts in coordination with two small G proteins (Ras1 and Ras2). Through comprehensive measurements of glucose-dependent transcription and metabolism, we demonstrate that the two receptor systems have distinct roles in glucose signaling: the G-protein-coupled receptor directs carbohydrate and energy metabolism, while the transceptors regulate ancillary processes such as ribosome, amino acids, cofactor and vitamin metabolism. The large G-protein transmits the signal from its cognate receptor, while the small G-protein Ras2 (but not Ras1) integrates responses from both receptor pathways. Collectively, our analysis reveals the molecular basis for glucose detection and the earliest events of glucose-dependent signal transduction in yeast.

Keywords: metabolomics; transcriptomics; G-protein-coupled receptor; transceptor; G protein; RAS; glucose; yeast

Citation: Li, S.; Li, Y.; Rushing, B.R.; Harris, S.E.; McRitchie, S.L.; Dominguez, D.; Sumner, S.J.; Dohlman, H.G. Multi-Omics Analysis of Multiple Glucose-Sensing Receptor Systems in Yeast. *Biomolecules* **2022**, *12*, 175. https://doi.org/10.3390/biom12020175

Academic Editors: James Konopka and Mark Rose

Received: 30 December 2021
Accepted: 18 January 2022
Published: 21 January 2022

1. Introduction

Most eukaryotic organisms use glucose as the principal source of carbon and energy. Changes in glucose availability result in important metabolic and transcriptional changes that dictate the transition between respiratory and fermentative metabolism [1–4]. Among the best understood systems is that of the yeast *Saccharomyces cerevisiae* (meaning "sugar fungus" and "beer"). Biochemical studies of yeast fermentation led to the discovery of enzymes (meaning "in yeast") and the founding of biochemistry as a distinct scientific discipline.

While the details of glucose metabolism are well understood, we know comparatively little about changes in signal transduction and cellular metabolism in response to glucose availability. These include changes attributed to glucose binding to cell surface receptors and activation of signaling pathways immediately downstream of the receptor but upstream of glycolysis. In this instance, an increase in glucose is transmitted by two distinct processes (Figure 1). In the first, glucose is detected by a G-protein-coupled receptor (GPCR) known as Gpr1 and transmitted through G protein α and β subunits, named Gpa2 and Asc1 respectively [5–13]. Glucose also activates the small G proteins Ras1 and Ras2, through the action of guanine nucleotide exchange factors [14–20]. In contrast to *ras2*Δ however, *ras1*Δ has no observed phenotype under standard laboratory growth

conditions [21]. Collectively [22–33], these proteins activate the effector enzyme adenylyl cyclase [24,34–36] leading to an increase in cellular cAMP [9,26,37]. This second messenger binds directly to protein kinase A, which goes on to phosphorylate multiple intracellular proteins involved in glucose uptake, metabolism and storage [38–44].

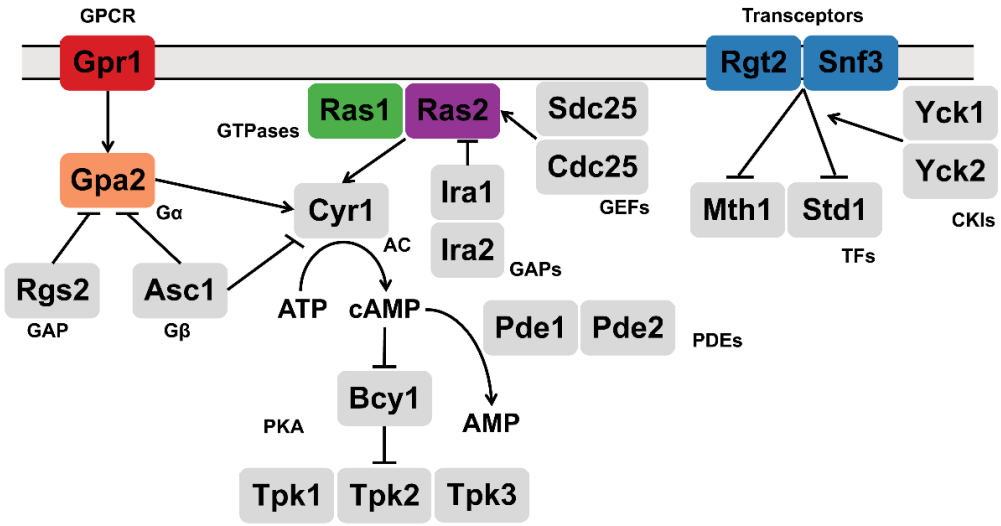

Figure 1. Glucose-sensing pathways in yeast. Two receptor pathways in *S. cerevisiae* respond to glucose availability. Gpr1 transmits its signal through the large G-protein Gpa2 [5–7,9–11] while Cdc25 and Sdc25 activate the small G-proteins Ras1 and Ras2. The transceptors Snf3 and Rgt2 recruit the protein kinases Yck1 and Yck2 as well as the transcription corepressors Mth1 and Std1 [45–49]. GPCR: G-protein coupled receptor; GAP: GTPase activating protein; GEF: guanine nucleotide exchange factor; AC: adenylyl cyclase; PDE: phosphodiesterase; TF: transcription factor; CKI: casein kinase I; PKA: protein kinase A.

The second glucose-sensing system consists of the cell surface proteins Snf3 and Rgt2. Although they resemble glucose transporters, Snf3 and Rgt2 appear to have lost their transporter function and instead serve exclusively as receptor or "transceptor" proteins. Following glucose addition [45–47], Snf3 and Rgt2 recruit the Type I casein kinases Yck1 and Yck2 as well as the transcription corepressors Mth1 and Std1 [48,49]. Subsequent phosphorylation of these factors results in their ubiquitination and degradation [50–52]; this derepresses genes encoding hexose transporters and promotes the uptake of the newly available sugars [47,53–62]. Here, we compare the function of the two glucose signaling pathways. In particular, we employ transcriptomics and metabolomics to provide a comprehensive view of the cellular response to glucose. Our analysis reveals new and complementary functions for the two glucose sensing receptors and an unexpected role for Ras2 as an integrator of these two receptor pathways.

2. Materials and Methods

2.1. Yeast Strains

The prototrophic (wildtype) strain used throughout was constructed from BY4741 (MATa *his3*Δ1 *leu2*Δ0 *met15*Δ0 *ura3*Δ0). *HIS3*, *LEU2*, *MET15* and *URA3* were integrated at the endogenous loci with sequence amplified by PCR from S288C strain DNA. All single mutants (*gpr1*Δ, *gpa2*Δ, *ras1*Δ, *ras2*Δ, *snf3*Δ *rgt2*Δ) were constructed by transforming the wildtype strain with corresponding sequence from the Yeast Knock-Out collection that replaces the target gene with KanMX4 [63]. The *snf3*Δ *rgt2*Δ double mutant was constructed by switching the mating type of *snf3* from MATa to MATα, with HO expressed from a plasmid, and then mating to an isogenic *rgt2* strain. The diploid was then sporulated and spore products with the *snf3*Δ *rgt2*Δ double knock-out were confirmed with PCR.

Cells maintained at 30 °C in Synthetic Complete (SC) (2% glucose) medium were centrifuged and washed twice and then resuspended into 10 mL SC (0.05% glucose) and

cultivated for 1 h. For high and low glucose treatment, 245 µL of 65.5% or 0.05% glucose was added to 10 mL cell culture respectively, each for exactly 2 min (metabolomics) or 10 min (transcriptomics). Subsequent analysis was performed as described previously [13], and as summarized below.

2.2. Sample Preparation for RNA-seq

500 µL of cell culture was centrifuged at 1000× *g* for 1 min at 4 °C; the resulting cell pellet was flash frozen by liquid nitrogen. Cells stored at −80 °C were resuspended with 600 µL buffer RLT 1% (*v*/*v*) 2-mercaptoethanol from the QIAGEN RNeasy Mini Kit (Cat No.: 74106), transferred to 2 mL OMNI prefilled ceramic bead tubes (SKU: 19-632), loaded onto an OMNI Bead Mill Homogenizer (SKU:19-040E) and agitated three times at 5 m/s for 1 min at 4 °C while cooled on ice for 3 min between each cycle. The resulting lysate was clarified by centrifugation at 11,000× *g* and used for total RNA extraction with QIAGEN RNeasy Mini Kit (Cat No.: 74106) with on-column DNase digestion. Extracted total RNA for each sample was evaluated for purity and quantified with the Qubit RNA HS Assay kit (Cat No.: Q32855) and an Invitrogen Qubit 2.0 Fluorometer (Cat No.: Q32866), each according to manufacturer's instructions.

RNA libraries were prepared with Kapa stranded mRNA-seq kits, with KAPA mRNA Capture Beads (KAPA code: KK8421; Roche Cat No.: 07962207001) through the UNC High Throughput Sequencing Facility. All procedures were according to manufacturer's instructions.

2.3. RNA Sequence Analysis

Quality of raw sequence was checked with the FASTQC algorithm (http://www.bioinformatics.babraham.ac.uk/projects/fastqc/, accessed on 29 July 2020). Sequence alignment to genome indices, generated based on *Saccharomyces cerevisiae* data downloaded from Ensembl.org, was performed with the STAR algorithm [64]. Quantification on the transcriptome level was performed with the SALMON algorithm [65]. Differences in transcript abundance were determined using a negative binomial generalized linear model in DESeq2 package in R [66,67]. Differentially Expressed Genes (DEGs) were defined as having adjusted *p*-value < 0.05, absolute log2 fold-change >1 and baseMean >100. A series of baseMean thresholds have been tested, including 0, 50 and 100. The conclusion remains unchanged. Therefore, the most stringent threshold (baseMean >100, which filters out >20% of genes) was chosen for data analysis.

PCA analysis was performed using the internal PCA function of DESeq2 package with variance stabilizing transformation (vst) normalized data.

2.4. Transcriptomics Pathway Enrichment Analysis and Over-Representation Analysis

Pathway enrichment analysis for transcriptomics data was performed with ClusterProfiler package in R [68]; Log2 fold-change for each comparison (mutantH vs. wtH) was extracted from corresponding DESeq2 analysis. GSEA analysis was then performed with gseKEGG function, with organism set to 'sce' (*Saccharomyces cerevisiae*), permutation number set to 1000, minimal and maximal size for each analyzed geneset as 3 and 200, *p*-value cutoff set to 0.05, *p*-value adjustment method set to 'BH' (Benjamini–Hochberg).

Over-representation analysis for the corresponding subsection of the Venn diagram was performed with the enrichKEGG function in the ClusterProfiler package, with organism set to 'sce' (*Saccharomyces cerevisiae*), minimal and maximal size for each analyzed geneset as 3 and 200, *p*-value cutoff set to 0.05, *p*-value adjustment method set to 'BH' (Benjamini–Hochberg).

2.5. Sample Preparation for Metabolomics

Three millilitres of cell culture was mixed with 45 mL cold pure methanol on dry ice and after 5 min centrifuged in a precooled rotor (−80 °C). Cell pellets were stored at −80 °C and resuspended with extraction reagent (8:2 methanol-water solution) to 3×10^8 cell/mL, transferred to 2 mL ceramic bead MagNalyser tubes and subjected to homogenization with Bead Ruptor Elite Bead Mill Homogenizer (OMNI International, Singapore) at 6.0 m/s for

40 s in two cycles at room temperature. This homogenization step was repeated twice. After centrifugation at 16,000× *g* for 10 min at 4 °C, 500 µL of the supernatant was transferred into low-bind 1.7 mL microfuge tubes. Total pools were made by combining an additional 65 µL of the supernatant from each sample and then aliquoting this mixture into low-bind 1.7 mL tubes at a volume of 500 µL. Samples and blanks were dried using a speedvac vacuum concentrator overnight. Following storage at −80 °C, samples were resuspended in 100 µL reconstitution buffer (95:5 water:methanol with 500 ng/mL tryptophan d-5), vortexed at 5000 rpm for 10 min, and then centrifuged at room temperature at 16,000× *g* for 4 min. Supernatant was transferred into autosampler vials for LC-MS.

2.6. UHPLC High-Resolution Orbitrap MS Metabolomics Data Acquisition

Metabolomics data were acquired on a Vanquish UHPLC system coupled to a QExactive HF-X Hybrid Quadrupole-Orbitrap Mass Spectrometer (ThermoFisher Scientific, San Jose, CA, USA), as described previously [69]. Our UPLC–MS reversed phase platform was established based on published methods [70,71]. Metabolites were separated using an HSS T3 C18 column (2.1 mm × 100 mm, 1.7 µm, Waters Corporation, Milford, MA, USA) at 50 °C with binary mobile phase of water (A) and methanol (B), each containing 0.1% formic acid (*v*/*v*). The UHPLC linear gradient started from 2% B, and increased to 100% B in 16 min, then held for 4 min, with the flow rate at 400 µL/min. The untargeted data were acquired in positive mode from 70 to 1050 m/z using the data-dependent acquisition mode.

2.7. Metabolomics Data Normalization and Filtration

Progenesis QI (version 2.1, Waters Corporation) was used for peak picking, alignment, and normalization as described previously [69]. Samples were randomized and run within two batches with blanks and pools interspersed at a rate of 10%. Starting from the unnormalized data for each of the batch runs, the data were filtered so as to only include signals with an average intensity fold change of 3.0 or greater in the total pools compared to the blanks. Individual samples (including pools, blanks, and study samples) were then normalized to a reference sample that was selected by Progenesis from the total pools via a function named "normalize to all". Signals were then excluded that were significantly different between pools of batch 1 and pools of batch 2 based on an ANOVA comparison calculated in Progenesis ($q < 0.05$). After normalization and filtration, 2397 signals passed the QC procedures and were used for further analysis.

The filtered and normalized data were mean-centered and Pareto-scaled prior to conducting the unsupervised principal component analysis using the ropls R package.

2.8. In-House Compound Identification and Annotation

Peaks were identified or annotated by Progenesis QI through matching to an in-house experimental standards library generated by acquiring data for approximately 1000 compounds under conditions identical to study samples, as well as to public databases (including HMDB, METLIN and NIST), as described previously [69]. Identifications and annotations were assigned using available data for retention time (RT), exact mass (MS), MS/MS fragmentation pattern, and isotopic ion pattern. The identification or annotation of each signal is provided in Supplementary Materials. Signals/metabolites that matched to the in-house experimental standards library by (a) RT, MS, and MS/MS are labeled as OL1, or (b) by RT and MS are labeled OL2a. An OL2b label was provided for signals that match by MS and MS/MS to the in-house library that were outside the retention time tolerance (±0.5 min) for the standards run under identical conditions. Signals matched to public databases are labeled as PDa (MS and experimental MS/MS), PDb (MS and theoretical MS/MS), PDc (MS and isotopic similarity or adducts), and PDd (MS only) are also provided (Supplementary Materials).

2.9. Compound Annotation, Metabolic Pathway Enrichment Analysis and Over-Representation Analysis

Compound annotation and pathway enrichment analysis for metabolomics was performed with the MetaboAnalystR 3.0 package in R [72,73] (https://www.metaboanalyst.ca/docs/RTutorial.xhtml, accessed on 5 June 2020). For compound annotations, molecular weight tolerance (ppm) was set to 3.0, analytical mode was set to positive and retention time was included. Pathway enrichment analysis was performed with the 'integ' module (using both Mummichog v2.0 and GSEA) with the yeast KEGG database. The *p*-value threshold for Mummichog was set at 0.05.

Normalized peak data from Progenesis QI were used as input for MetaboAnalystR. The interaction term estimated how the response amplitude of each mutant is different from wildtype, which is (mutantH-mutantL)-(wtH-wtL). The modeled *p*-value and t score for the interaction term associated with each peak were then used as inputs for pathway enrichment analysis. Significantly perturbed metabolites (SPMs) were defined as annotations that have adjusted *p*-value < 0.05 (FDR) from the output of MetaboAnalystR. Significantly perturbed pathways were defined as having combined *p*-value < 0.05 (Mummichog and GSEA).

Over-representation analysis for the corresponding subsection of the Venn diagram was performed with the Enrichment Analysis module in MetaboAnalystR, with KEGG ID for each metabolite as the input. FDR adjusted *p*-value < 0.05 was the threshold for over-represented pathways.

2.10. Integration of Transcriptomics and Metabolomics Data

Integration analysis was performed with the 'joint pathway analysis' module of MetaboAnalystR (https://www.metaboanalyst.ca/docs/RTutorial.xhtml, accessed on 20 November 2020). Gene input together with log2 fold-change was generated based on the corresponding DESeq2 analysis, with the threshold set as adjusted *p*-value < 0.05, absolute log2 fold-change >1 and baseMean >100 (DEGs); metabolite input together with log2 fold-change was generated based on MetaboAnalystR analysis, with the threshold set as adjusted *p*-value < 0.05 (SPMs). Integration analysis was performed on 'all pathways', which includes both metabolic pathways as well as gene-only pathways. Enrichment analysis was performed using 'Hypergeometric test'. Topology measure was set to 'Degree Centrality'. Integration method was set to 'combine queries', which is a tight integration method with genes and metabolites pooled into a single query and used to perform enrichment analysis within their "pooled universe". Significantly enriched pathways were defined as having FDR adjusted *p*-value < 0.05.

2.11. Yeast RNA Extraction, DNase Treatment, and Reverse Transcription for qPCR

RNA was extracted from cells using hot acid phenol. TES solution (10 mM Tris-HCl, pH 7.5; 10 mM EDTA; 0.5% SDS) was used to resuspend pellets then the resuspension was incubated for one hour at 65 °C. The RNA was separated via phenol-chloroform extraction and any residual DNA was degraded with RQ1 DNase (Promega, Madison, WI, USA). To further purify the RNA, RNeasy mini kit (Qiagen, Frederick, MD, USA) was used and the final RNA concentration was determined via spectrophotometry with a NanoDrop One (ThermoFisher Scientific, Waltham, MA, USA). cDNA was produced via reverse transcription from 250 ng RNA using a High-Capacity cDNA Reverse Transcription Kit (ThermoFisher Scientific) following manufacturer's protocol.

2.12. qPCR

qPCR primers were ordered from Integrated DNA Technologies:

YER100W_FWD primer	5′ GAAGCCACGACAGGATCAAT 3′
YER100W_REV primer	5′ ATCCCCCTCATCCAATTTTC 3′
YBR117C_FWD	5′ GTCACTCATGCGCTCTTCTG 3′
YBR117C_REV	5′ GAGTCGGAAATGGGAAAGCC 3′
YPL061W_FWD	5′ GGCGCCAAGATCTTAACTGG 3′
YPL061W_REV	5′ CCACCTTCAAACCTGTGCTC 3′
YJL153C_FWD	5′ CATGGTTAGCCCAAACGACT 3′
YJL153C_REV	5′ CGTGGTTACGTTGCCTTTTT 3′
YFL030W_FWD	5′ TGATCCCAGGCCCCATTATC 3′
YFL030W_REV	5′ AATATGTCCCACCCCAACGT 3′

To perform qPCR, cDNA was diluted 50-fold and amplified with SsoAdvanced Universal SYBR Green Supermix (Bio-Rad, Hercules, CA, USA) following manufacturer's protocols with adjustments: 45 cycles were used to increase amplification and anneal/extension time was extended to 45 s. qPCR was performed in technical triplicate for each of the six biological replicates per genotype. CFX Maestro Software (Bio-Rad) was used to determine the threshold cycle (C_t). ΔC_t values were determined in reference to YER100W and final $\Delta\Delta C_t$ values were calculated and normalized in reference to wildtype cells. *p*-values were calculated on ΔC_t values between genotypes via independent, non-parametric, one-tailed Mann–Whitney U tests with the expected change in expression as was found by RNAseq. One exception was that of *TKL2* in *snf3*Δ *rgt2*Δ vs. wildtype comparison in which the RNAseq data did not yield a statistically significant change, in this case, a two-sided Mann–Whitney U-test was applied. The Benjamini–Hochberg Procedure was used to correct for multiple comparisons.

3. Results

3.1. Unsupervised Principal Component Analysis (PCA)

It is well established that yeast employs two different receptor systems in response to glucose. To investigate the impact of each receptor system, we used untargeted transcriptomics and metabolomics on wildtype cells and mutants lacking the GPCR Gpr1, the large G protein Gpa2, the small G proteins Ras1 or Ras2, or the transceptors Snf3 and Rgt2, under high or low glucose conditions. Log phase wildtype and mutant cells (all prototrophic) were grown for 1 h in low (L, 0.05%) glucose, then divided and either left untreated or treated with high (H, 2%) glucose for 2 min (metabolomics) or 10 min (transcriptomics). These time points were selected based on prior data, showing an early and transient spike of cAMP and a subsequent induction of genes within 10 min of glucose treatment [1,13].

Principal Component Analysis (PCA) is an unsupervised multivariate analysis method useful for the visualization of the relationship between observations and variables. When applied to our transcriptomics data, PCA revealed good differentiation based on the proximity of data points for a given treatment and genotype (Figure S1a). This analysis revealed that PC1, which aligns primarily with treatment, accounts for 89% of variance while PC2, which aligns primarily with genotype, represents 4% of variance. Thus, the first 2 components explained 93% of the variance. For metabolomics, the first 2 components explained 50% of the variance (Figure S1b). With the exception of *ras1*Δ, the mutants were distant from wildtype in both measurements. While *gpr1*Δ aligned closely with *gpa2*Δ, *snf3*Δ *rgt2*Δ was on the opposite side of wildtype. The *ras2*Δ mutant was located between the two receptor mutants. These measures indicate distinct effects of the two receptor systems, and a potential role for Ras2 in both.

3.2. Glucose Sensing in Wildtype Cells

Glucose has multiple and complex effects on metabolism and gene expression. To validate our approach, we first performed pathway enrichment analysis, comparing high and low glucose in wildtype cells. For transcriptomics we used the ClusterProfiler package

in R [68] and performed gene set enrichment analysis (GSEA) with the Kyoto Encyclopedia of Genes and Genomes (KEGG) database [74–76]. As expected, perturbed pathways were mainly associated with carbohydrate, amino acids, lipids and nucleotide metabolism as well as transcription, ribosome, replication, and cell cycle pathways (See Table 1 in [13], reproduced in Table S1). These pathways are important for cell growth following the addition of glucose [77]. For metabolomics we used MetaboAnalystR, which integrates the results of Mummichog and GSEA, to produce the combined *p*-values reported for each pathway (See Table 1 in [13] reproduced in Table S1) [72,73,78]. We identified enrichment in six pathways associated with metabolism of carbohydrates, amino acids, and lipids, which is consistent with our transcriptomics analysis. Below we elaborate on how the two receptor systems function individually and in relation to one another.

Table 1. Single- and multi-omics integration results for *gpr1*Δ. The first block shows GSEA for transcriptomics with adjusted *p*-value < 0.05, arranged in ascending order; second block shows MetaboAnalystR pathway enrichment analysis for metabolomics with combined *p*-value < 0.05, arranged in ascending order; third block shows MetaboAnalystR joint pathway analysis with adjusted *p*-value < 0.05, arranged in ascending order, as detailed in the methods.

Transcriptomics		Metabolomics		Integration	
Enriched Pathways	**Adjusted *p*-Value**	**Enriched Pathways**	**Combined *p*-Value**	**Enriched Pathways**	**Adjusted *p*-Value**
Oxidative phosphorylation	0.0082	Fructose and mannose metabolism	0.0021	Oxidative phosphorylation	5.24×10^{-19}
Starch and sucrose metabolism	0.0082	Purine metabolism	0.0034	Galactose metabolism	8.60×10^{-13}
		Amino sugar and nucleotide sugar metabolism	0.0075	Starch and sucrose metabolism	6.56×10^{-10}
		Galactose metabolism	0.0075	ABC transporters	7.22×10^{-8}
		Tyrosine metabolism	0.0090	Glycolysis or Gluconeogenesis	1.75×10^{-7}
		Glutathione metabolism	0.0107	Arginine biosynthesis	5.76×10^{-5}
		Lysine biosynthesis	0.0177	Alanine, aspartate and glutamate metabolism	0.0001
		Arginine biosynthesis	0.0229	Purine metabolism	0.0001
		Butanoate metabolism	0.0375	Citrate cycle (TCA cycle)	0.0001
				Fructose and mannose metabolism	0.0003
				Amino sugar and nucleotide sugar metabolism	0.0009
				Cysteine and methionine metabolism	0.0025
				Pentose phosphate pathway	0.0025
				Nitrogen metabolism	0.0128
				beta-Alanine metabolism	0.0128
				Glycine, serine and threonine metabolism	0.0175
				Pyruvate metabolism	0.0264
				Glutathione metabolism	0.0266

3.3. Comparison of Glucose Signaling by the GPCR and Transceptor Systems

Transcriptomics analysis. We next determined the transcriptional response to high glucose, comparing wildtype cells with mutants lacking the GPCR (*gpr1*Δ), or the two transceptors (*snf3*Δ *rgt2*Δ). In comparison to wildtype, *gpr1*Δ affected pathways related to oxidative

phosphorylation as well as starch and sucrose metabolism, both of which are centered on carbohydrate utilization and energy metabolism (Tables 1 and S2). In comparison to wildtype, *snf3*Δ *rgt2*Δ affected pathways related to RNA polymerase, ribosome, autophagy and amino acid metabolism, which are centered on nitrogen utilization and translation (Tables 2 and S3). Thus, under high glucose conditions, the GPCR and transceptor pathways primarily regulate carbohydrate and amino acid metabolism, respectively.

Table 2. Single- and multi-omics integration results for *snf3*Δ *rgt2*Δ. First block shows GSEA for transcriptomics with adjusted *p*-value < 0.05, arranged in ascending order; second block shows MetaboAnalystR pathway enrichment analysis for metabolomics with combined *p*-value < 0.05, arranged in ascending order; third block shows MetaboAnalystR joint pathway analysis with adjusted *p*-value < 0.05, arranged in ascending order, as detailed in the Methods.

Transcriptomics		Metabolomics		Integration	
Enriched Pathways	**Adjusted *p*-Value**	**Enriched Pathways**	**Combined *p*-Value**	**Enriched Pathways**	**Adjusted *p*-Value**
Ribosome	0.0076	Purine metabolism	0.0005	Ribosome	1.12×10^{-74}
Ribosome biogenesis in eukaryotes	0.0076	Arginine biosynthesis	0.0026	Purine metabolism	1.76×10^{-9}
Sulfur metabolism	0.0076	Cysteine and methionine metabolism	0.0027	Longevity regulating pathway	9.20×10^{-6}
RNA polymerase	0.0154	Glyoxylate and dicarboxylate metabolism	0.0055	Alanine, aspartate and glutamate metabolism	2.05×10^{-5}
Nitrogen metabolism	0.0165	Glycine, serine and threonine metabolism	0.0085	Arginine biosynthesis	0.0004
Autophagy	0.0165	Taurine and hypotaurine metabolism	0.0172	Glycine, serine and threonine metabolism	0.0006
Alanine, aspartate and glutamate metabolism	0.0289	Glutathione metabolism	0.0174	Glycolysis or Gluconeogenesis	0.0049
Proteasome	0.0465	Methane metabolism	0.0254	Starch and sucrose metabolism	0.0080
				Cysteine and methionine metabolism	0.0088
				One carbon pool by folate	0.0174
				Glyoxylate and dicarboxylate metabolism	0.0174
				Sulfur metabolism	0.0193
				Pyruvate metabolism	0.0193
				Histidine metabolism	0.0193
				Galactose metabolism	0.0261
				Peroxisome	0.0295
				Glycerolipid metabolism	0.0392

We then performed over-representation analysis (ORA) for differentially expressed genes (DEGs), comparing *gpr1*Δ vs. wildtype and *snf3*Δ *rgt2*Δ vs. wild-type, both under high glucose conditions. In each case, we defined the DEGs as having an adjusted *p*-value < 0.05, absolute log2 fold-change value >1 and baseMean >100. Whereas GSEA is a type of functional class scoring that considers a complete list of ranked items (all gene transcripts in this application), ORA considers a thresholded subset of items (DEGs, defined above). In this way, we were able to gain a detailed understanding of how the mutants are similar and how they differ from one another. Figure 2a shows a Venn diagram comparing the specific DEGs for each mutant vs. the wildtype strain (Table S4). As shown in Figure 2b, DEGs unique to *gpr1*Δ were primarily related to carbohydrate and energy metabolism, consistent with Gpr1's function as a sensor of glucose availability. DEGs unique to *snf3*Δ *rgt2*Δ were mainly related to ribosome, purine, cofactor and vitamin

metabolism (Figure 2c). While the two mutant strains had concordant effects on some DEGs (Figure 2d), they had—contrary to our expectations—substantial and opposing effects on a broad set of DEGs primarily related to carbohydrate and amino acid metabolism (Figure 2e). Thus, GSEA and ORA are in agreement, and indicate that the two receptor pathways are largely distinct. When the pathways converge on a shared set of carbohydrate- and amino acid-related transcripts (DEGs), they do so largely in opposition to one another.

a

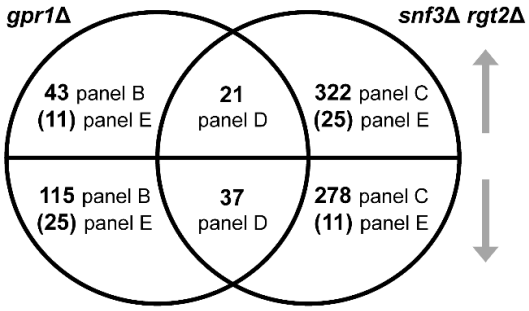

b

pathways	adjusted p-value	functional category
Oxidative phosphorylation	5.57×10^{-19}	Energy
Starch and sucrose metabolism	9.68×10^{-5}	Carbohydrate
Carbon metabolism	0.0151	Carbohydrate
Glycolysis / Gluconeogenesis	0.0213	Carbohydrate
Citrate cycle (TCA cycle)	0.0283	Carbohydrate
Amino sugar and nucleotide sugar metabolism	0.0358	Carbohydrate
Fatty acid metabolism	0.0414	Lipid
Galactose metabolism	0.0422	Carbohydrate
Fatty acid biosynthesis	0.0422	Lipid
Riboflavin metabolism	0.0472	Cofactors and vitamins

c

pathways	adjusted p-value	functional category
Ribosome	3.04×10^{-59}	Genetic information processing
Longevity regulating pathway	0.0004	Organismal systems
Purine metabolism	0.0005	Nucleotide
Sulfur metabolism	0.0050	Energy
One carbon pool by folate	0.0281	Cofactors and vitamins
Biosynthesis of cofactors	0.0451	Cofactors and vitamins

d

pathways	adjusted p-value	functional category
Steroid biosynthesis	0.0332	Lipid
Biosynthesis of amino acids	0.0380	Amino acid
Nitrogen metabolism	0.0392	Energy

e

pathways	adjusted p-value	functional category
Pyruvate metabolism	0.0137	Carbohydrate
Glycolysis / Gluconeogenesis	0.0137	Carbohydrate
Carbon metabolism	0.0152	Carbohydrate
Citrate cycle (TCA cycle)	0.0152	Carbohydrate
Ascorbate and aldarate metabolism	0.0231	Carbohydrate
beta-Alanine metabolism	0.0236	Carbohydrate
Valine, leucine and isoleucine degradation	0.0236	Amino acid
Histidine metabolism	0.0236	Amino acid
Lysine degradation	0.0274	Amino acid
Fatty acid degradation	0.0348	Lipid
Tryptophan metabolism	0.0348	Amino acid
Arginine and proline metabolism	0.0386	Amino acid
Pantothenate and CoA biosynthesis	0.0386	Cofactors and vitamins

Figure 2. Comparing differentially expressed genes (DEGs) of *gpr1*Δ and *snf3*Δ *rgt2*Δ. (**a**) Venn diagram of subsets of DEGs, for *gpr1*Δ vs. wildtype and *snf3*Δ *rgt2*Δ vs. wildtype, after glucose addition to 2%. Upper semicircle shows up-regulated DEGs and lower semicircle shows down-regulated DEGs. Numbers in the overlapping region are shared DEGs regulated in the same direction. Numbers in parenthesis are shared DEGs regulated in the opposite direction, and are placed in the area corresponding to the direction of regulation. DEGs used for ORA analysis that are (**b**) unique to *gpr1*Δ; (**c**) unique to *snf3*Δ *rgt2*Δ; (**d**) shared and change in the same direction; (**e**) shared and change in the opposite direction. Listed are all pathways and their functional categories with adjusted p-value < 0.05.

Metabolomics analysis. Gene transcription is regulated by, and in turn regulates, complex metabolic processes in the cell. To better understand the relationship of these two glucose-sensing systems, we examined the role of each receptor type after glucose addition, and did so using untargeted metabolomics. Based on MetaboAnalystR, our mass spectrometry data show that the *gpr1*Δ cells were enriched in nine pathways related to carbohydrate and amino acid metabolism (Tables 1 and S2), while *snf3*Δ *rgt2*Δ cells were enriched in eight pathways, including those related to amino acid and purine metabolism, but not central carbohydrate metabolism (Tables 2 and S3). A Venn diagram shows shared and

unique metabolites that were significantly perturbed in each strain (Figure 3a and Table S5). Values were obtained from the output of MetaboAnalystR and represent annotations with adjusted *p*-value < 0.05. These are hereafter referred to as significantly perturbed metabolites (SPMs). ORA revealed that several purine metabolites changed in the same direction (Figure 3b) while a substantial number of carbohydrate metabolites changed in the opposite direction (Figure 3c). As expected, the signals identified and annotated by MetaboAnalyst mirror those obtained using in-house library annotation, developed with data acquired for standards run under the same conditions as the study samples, as well as matching to public databases (PD), as described in our companion manuscript [13], and reported in Table S6. Subsequent analysis relied on MetaboAnalystR, which is well-suited for annotating a large number of signals.

a

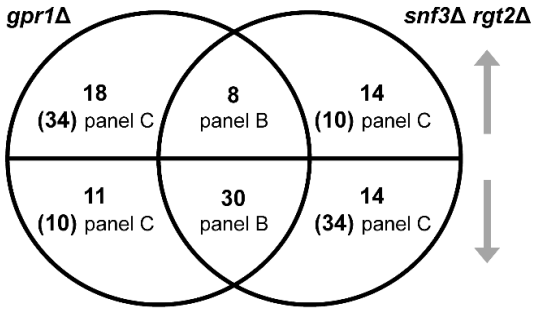

b

pathways	adjusted p-value	functional category
Purine metabolism	3.19×10^{-6}	Nucleotide

c

pathways	adjusted p-value	functional category
Fructose and mannose metabolism	9.16×10^{-5}	Carbohydrate
Amino sugar and nucleotide sugar metabolism	0.0003	Carbohydrate

Figure 3. Comparing significantly perturbed metabolites (SPMs) of *gpr1*Δ and *snf3*Δ *rgt2*Δ. (**a**) Venn diagram of subsets of SPMs, for *gpr1*Δ vs. wildtype and *snf3*Δ *rgt2*Δ vs. wildtype, after glucose addition. Upper semicircle shows up-regulated SPMs and lower semicircle shows down-regulated SPMs. Numbers in the overlapping region are shared SPMs regulated in the same direction. Numbers in parenthesis are shared SPMs regulated in the opposite direction, and are placed in the area corresponding to the direction of regulation. SPMs used for ORA analysis that are (**b**) shared and change in the same direction; (**c**) shared and change in the opposite direction. Listed are all pathways and their functional categories with adjusted *p*-value < 0.05.

Integration analysis. Our analysis above shows that the GPCR Gpr1 regulates carbohydrate metabolism while the transceptors Snf3 and Rgt2 regulate ribosome, amino acid, cofactor and vitamin metabolism. Effects that are shared but opposing are primarily related to carbohydrate metabolism; however, these represent only a small subset of the DEGs and SPMs affected by Snf3 and Rgt2. In general, and to our surprise, the glucose transceptors did little to regulate the metabolism of glucose and other sugars. This is most likely because we measured changes after ten minutes, while past studies measured changes after longer treatments. We infer that the transceptors are involved in longer term effects on carbohydrate metabolism. To gain a deeper understanding of the functional relationship between changes in gene transcription and host metabolites, we employed the joint pathway analysis module in MetaboAnalystR, as described previously [13,72,73]. In this application, we input all DEGs (transcriptomics) and SPMs (metabolomics) and queried for those over-represented in KEGG. By integrating the data in this manner, we increased the power of our analysis and were able to obtain more information than could be gleaned from transcriptomics or metabolomics alone. Once again, we found that Gpr1 primarily regulates carbohydrate and energy metabolism (Tables 1 and S2) while Snf3 and Rgt2 primarily regulate the ribosome, amino acids, lipids and cofactor metabolism (Tables 2 and S3). Both receptor systems affect genes or metabolites involved in carbohydrates, amino acids and purine metabolites. Thus, integration analysis confirms what we observed on the single-omics level: Gpr1 is primarily dedicated to carbohydrate metabolism while Snf3 and Rgt2 work to coordinate other species in response to glucose addition.

To visualize the functional relationship of the two receptor systems, we projected the inputs of our integration analysis onto the pertinent yeast metabolic pathways in KEGG. From this projection it was evident that the two receptor types regulate distinct and complementary processes. Specifically, Gpr1 affects pathways related to carbohydrate metabolism and, within those pathways, a larger number of genes and metabolites compared to Snf3 and Rgt2 (Figures 4a and S2 and Tables 1 and 2). On the other hand, Snf3 and Rgt2 affect pathways related to amino acids and, within those pathways, affect a far greater number of genes and metabolites in comparison to Gpr1 (Figures 4b and S3 and Tables 1 and 2). As presented from the single-omics analysis above, the shared effects on carbohydrate and amino acids were mostly antagonistic while the shared effects on purines were concordant.

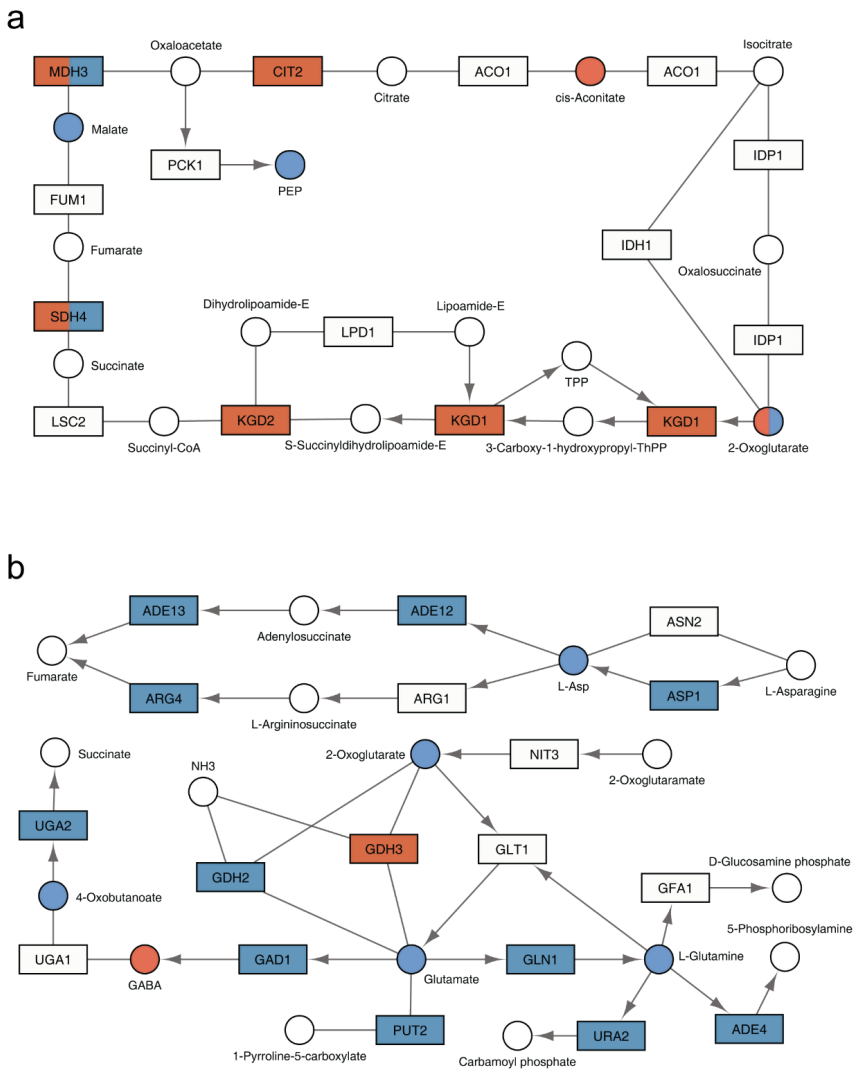

Figure 4. KEGG pathways regulated by *GPR1* or *SNF3* and *RGT2*. Regions of interest in the KEGG pathway are shown with genes displayed as rectangles and metabolites displayed as circles. KEGG compound name for each metabolite is labeled beside the circle. Standard gene names are labeled inside the rectangle. For enzyme complexes, the gene name for the major component is shown followed with an ellipsis. The directions of irreversible enzymatic reactions are shown by the arrows. Reversible reactions are connected by straight lines. DEGs and SPMs are highlighted in red (*gpr1*Δ) and blue (*snf3*Δ *rgt2*Δ). Shared DEGs and SPMs are colored half red and half blue. (**a**) as compared with *snf3*Δ *rgt2*Δ, *gpr1*Δ affected more components in citrate cycle (TCA cycle, functional category: carbohydrate); (**b**) as compared with *gpr1*Δ, *snf3*Δ *rgt2*Δ affected more components in alanine, aspartate and glutamate metabolism (showing aspartate and glutamate specifically, functional category: amino acid).

In summary, our transcriptomics and metabolomics pipeline established a distinct role for each receptor. Two minutes after sugar addition the GPCR and transceptors have opposing effects on many of the same metabolites (Figure 3). After ten minutes however, they confer changes on a largely different set of gene transcripts (Figure 2): whereas the effects of Gpr1 are mostly limited to genes controlling carbohydrate metabolism, Snf3 and Rgt2 affect more diverse species, including genes that are related to amino acids, lipids, ribosome, cofactors and vitamins. These differences could be the cause, or consequence, of reduced growth under glucose limiting conditions. Snf3 and Rgt2 do little to alter carbohydrate metabolism, and any changes that do occur are largely in opposition to Gpr1. Such antagonistic effects may allow the cell to fine-tune responses and to optimize temporal control of enzyme activities.

3.4. Comparison of Glucose Signaling through Large and Small G Proteins

Gpr1 acts through a G protein comprised of an α subunit Gpa2 and an atypical Gβ subunit Asc1 [6–9,12]. In parallel, guanine nucleotide exchange factors (Cdc25 and Sdc25) activate the small G proteins Ras1 and Ras2 [14–20]. Somewhat paradoxically, deletion of Gpr1 or Gpa2 also leads to the activation of Ras2 [79]. These opposing effects may be mediated by Asc1 [13]. Our recent analysis of Gpa2 and Asc1 revealed that they have mostly opposing effects on transcripts and metabolites. When the effects are congruent however, they mirror those observed for their shared activator Gpr1 [13]. To better understand how the receptors transmit their signals in response to glucose addition, we next compared the function of the large and small G proteins (Gpa2, Ras1 and Ras2) using the same analytical pipeline as described above.

Transcriptomics Analysis. We began by determining the transcriptional profiles of individual gene deletion mutants, by GSEA as described above. The *ras1*Δ mutant yielded no DEGs, consistent with the lack of phenotype for *ras1*Δ in standard laboratory growth conditions [21]. As shown in Tables 3 and 4 (also Tables S7 and S8), the *gpa2*Δ mutant affected pathways related to oxidative phosphorylation and ribosome biogenesis. These pathways were likewise regulated by *ras2*Δ. In addition, *ras2*Δ affected RNA polymerase, carbohydrate metabolism and autophagy (Table 4). Overlap between the large and small G proteins was expected given that both are activators of adenylyl cyclase. However, based on the Venn diagram, these mutants had correspondent effects on only a small number of genes and opposing effects on even fewer (Figure 5a and Table S9). Based on ORA, for the small number of shared DEGs, *gpa2*Δ and *ras2*Δ had mostly concordant effects on processes related to carbohydrate, amino acid and lipid metabolism (Figure 5b). DEGs unique to *ras2*Δ affected a broad spectrum of processes, encompassing all major species in KEGG, including the metabolism of energy, carbohydrates, amino acids, nucleotides, lipids, cofactors and vitamins (Figure 5c). In contrast, DEGs unique to *gpa2*Δ affected a small number of processes, related to carbohydrate, energy and lipid metabolism (Figure 5d). Thus, upon glucose addition, Gpa2 regulates carbohydrates and lipids, while Ras2 affects all major categories of metabolic processes.

Table 3. Single- and multi-omics integration results for *gpa2*Δ. First block shows GSEA for transcriptomics with adjusted *p*-value < 0.05, arranged in ascending order; second block shows MetaboAnalystR pathway enrichment analysis for metabolomics with combined *p*-value < 0.05, arranged in ascending order; third block shows MetaboAnalystR joint pathway analysis with adjusted *p*-value < 0.05, arranged in ascending order, as detailed in Methods.

Transcriptomics		Metabolomics		Integration	
Enriched Pathways	**Adjusted *p*-Value**	**Enriched Pathways**	**Combined *p*-Value**	**Enriched Pathways**	**Adjusted *p*-Value**
Ribosome biogenesis in eukaryotes	0.0084	Purine metabolism	0.0021	Oxidative phosphorylation	3.13×10^{-14}
Oxidative phosphorylation	0.0084	Fructose and mannose metabolism	0.0047	Galactose metabolism	1.60×10^{-11}

Table 3. *Cont.*

Transcriptomics		Metabolomics		Integration	
Enriched Pathways	**Adjusted *p*-Value**	**Enriched Pathways**	**Combined *p*-Value**	**Enriched Pathways**	**Adjusted *p*-Value**
		Amino sugar and nucleotide sugar metabolism	0.0079	ABC transporters	1.31×10^{-8}
		Galactose metabolism	0.0079	Glycolysis or Gluconeogenesis	8.02×10^{-5}
		Glutathione metabolism	0.0155	Fructose and mannose metabolism	8.18×10^{-5}
		Tyrosine metabolism	0.0224	Starch and sucrose metabolism	8.18×10^{-5}
		Arginine biosynthesis	0.0234	Arginine biosynthesis	0.0012
		Biotin metabolism	0.0252	Pentose phosphate pathway	0.0012
		Aminoacyl-tRNA biosynthesis	0.0360	Purine metabolism	0.0017
		Starch and sucrose metabolism	0.0396	Amino sugar and nucleotide sugar metabolism	0.0073
		Phosphatidylinositol signaling system	0.0424	beta-Alanine metabolism	0.0119
				Alanine, aspartate and glutamate metabolism	0.0139
				Cysteine and methionine metabolism	0.0149
				Citrate cycle (TCA cycle)	0.0221

Table 4. Single- and multi-omics integration results for *ras2*Δ. First block shows GSEA for transcriptomics with adjusted *p*-value < 0.05, arranged in ascending order; second block shows MetaboAnalystR pathway enrichment analysis for metabolomics with combined *p*-value < 0.05, arranged in ascending order; third block shows MetaboAnalystR joint pathway analysis with adjusted *p*-value < 0.05, arranged in ascending order, as detailed in Methods.

Transcriptomics		Metabolomics		Integration	
Enriched Pathways	**Adjusted *p*-Value**	**Enriched Pathways**	**Combined *p*-Value**	**Enriched Pathways**	**Adjusted *p*-Value**
Starch and sucrose metabolism	0.0065	Lysine biosynthesis	1.00×10^{-5}	Galactose metabolism	1.24×10^{-15}
Oxidative phosphorylation	0.0065	Glyoxylate and dicarboxylate metabolism	0.0005	Starch and sucrose metabolism	1.68×10^{-11}
Ribosome biogenesis in eukaryotes	0.0065	Glycine, serine and threonine metabolism	0.0009	Glycolysis or Gluconeogenesis	6.26×10^{-8}
Ribosome	0.0065	Arginine biosynthesis	0.0017	Glycine, serine and threonine metabolism	4.30×10^{-6}
RNA polymerase	0.0092	Cysteine and methionine metabolism	0.0028	ABC transporters	1.03×10^{-5}
Galactose metabolism	0.0169	Taurine and hypotaurine metabolism	0.0043	Pentose phosphate pathway	2.27×10^{-5}
Autophagy	0.0169	Amino sugar and nucleotide sugar metabolism	0.0043	Cysteine and methionine metabolism	2.27×10^{-5}
Meiosis	0.0332	Galactose metabolism	0.0043	Fructose and mannose metabolism	0.0002
Spliceosome	0.0458	Butanoate metabolism	0.0095	Amino sugar and nucleotide sugar metabolism	0.0002
		Lysine degradation	0.0098	Arginine biosynthesis	0.0003
		Aminoacyl-tRNA biosynthesis	0.0098	Purine metabolism	0.0005
		Starch and sucrose metabolism	0.0204	Glyoxylate and dicarboxylate metabolism	0.0009
		Alanine, aspartate and glutamate metabolism	0.0372	Peroxisome	0.0014
		Fructose and mannose metabolism	0.0384	Methane metabolism	0.0057
		Nitrogen metabolism	0.0392	Alanine, aspartate and glutamate metabolism	0.0057
		Phosphatidylinositol signaling system	0.0429	Lysine biosynthesis	0.0213
				Nitrogen metabolism	0.0255
				Citrate cycle (TCA cycle)	0.0338
				Vitamin B6 metabolism	0.0385
				Inositol phosphate metabolism	0.0390
				Monobactam biosynthesis	0.0392
				Tryptophan metabolism	0.0464

a

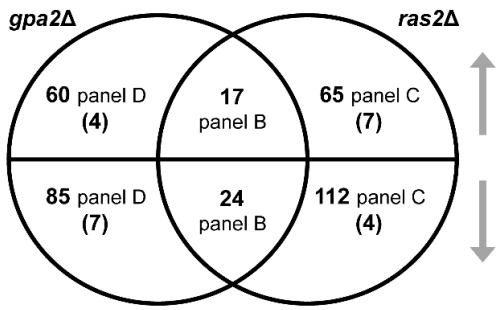

b

pathways	adjusted p-value	functional category
Starch and sucrose metabolism	0.0221	Carbohydrate
Histidine metabolism	0.0221	Amino acid
Pyruvate metabolism	0.0221	Carbohydrate
Carbon metabolism	0.0221	Carbohydrate
Glycolysis / Gluconeogenesis	0.0221	Carbohydrate
Fatty acid degradation	0.0258	Lipid
Tryptophan metabolism	0.0258	Amino acid
Arginine and proline metabolism	0.0298	Amino acid
Pentose phosphate pathway	0.0389	Carbohydrate

c

pathways	adjusted p-value	functional category
Carbon metabolism	0.0019	Carbohydrate
Starch and sucrose metabolism	0.0020	Carbohydrate
Nitrogen metabolism	0.0020	Energy
Glycine, serine and threonine metabolism	0.0080	Amino acid
Cysteine and methionine metabolism	0.0080	Amino acid
Biosynthesis of amino acids	0.0128	Amino acid
Methane metabolism	0.0165	Energy
Biosynthesis of cofactors	0.0165	Cofactors and vitamins
Peroxisome	0.0173	Cellular processes
Purine metabolism	0.0221	Nucleotide
Fatty acid degradation	0.0271	Lipid
Galactose metabolism	0.0473	Carbohydrate
Vitamin B6 metabolism	0.0473	Cofactors and vitamins

d

pathways	adjusted p-value	functional category
Oxidative phosphorylation	2.23×10^{-16}	Energy
Citrate cycle (TCA cycle)	0.0233	Carbohydrate
Fatty acid metabolism	0.0394	Lipid
Fatty acid biosynthesis	0.0474	Lipid

Figure 5. Comparing differentially expressed genes (DEGs) of *gpa2*Δ and *ras2*Δ. (**a**) Venn diagram of subsets of DEGs, for *gpa2*Δ vs. wildtype and *ras2*Δ vs. wildtype, after glucose addition to 2%. Upper semicircle shows up-regulated DEGs and lower semicircle shows down-regulated DEGs. Numbers in the overlapping region are shared DEGs regulated in the same direction. Numbers in parenthesis are shared DEGs regulated in the opposite direction, and are placed in the area corresponding to the direction of regulation. DEGs used for ORA analysis that are (**b**) shared and change in the same direction; (**c**) unique to *ras2*Δ; (**d**) unique to *gpa2*Δ. Listed are all pathways and their functional categories with adjusted *p*-value < 0.05.

Metabolomics Analysis. To better understand the relationship of large and small G proteins, we next conducted untargeted metabolomics on the corresponding mutants after glucose addition. Again, we used MetaboAnalystR for pathway enrichment analysis. In agreement with our transcriptomics data, we found that *gpa2*Δ and *ras2*Δ affected several common pathways related to carbohydrate and amino acid metabolism; however, *ras2*Δ impacted a wider variety of amino acid species (Tables 3 and 4, Tables S7 and S8). Based on the Venn diagram and ORA analysis, *gpa2*Δ and *ras2*Δ had a large number of shared SPMs that changed in the same direction, most of which were related to carbohydrate metabolism (Figure 6 and Table S10). In summary, two minutes after sugar addition the *gpa2*Δ and *ras2*Δ strains exhibited a similar metabolic profile (Figure 6). However, after ten minutes, *gpa2*Δ and *ras2*Δ exhibited a different transcriptional profile (Figure 5): while *gpa2*Δ mainly affected transcripts related to carbohydrates and lipids, *ras2*Δ impacted transcripts related to all major categories of metabolic processes. By any measure, the *ras1*Δ mutant yielded no significant differences, at least under the experimental conditions used in this analysis.

a

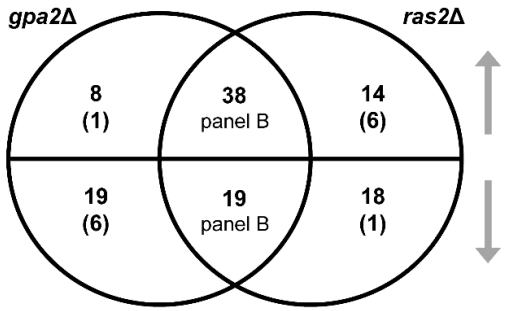

b

pathways	adjusted p-value	functional category
Galactose metabolism	2.09×10^{-8}	Carbohydrate
Amino sugar and nucleotide sugar metabolism	9.02×10^{-8}	Carbohydrate
Fructose and mannose metabolism	1.01×10^{-5}	Carbohydrate
Starch and sucrose metabolism	0.0033	Carbohydrate
Glycolysis / Gluconeogenesis	0.0442	Carbohydrate

Figure 6. Comparing significantly perturbed metabolites (SPMs) of *gpa2*Δ and *ras2*Δ. (**a**) Venn diagram of subsets of SPMs, for *gpa2*Δ and *ras2*Δ vs. wildtype, after glucose addition. Upper semicircle shows up-regulated SPMs and lower semicircle shows down-regulated SPMs. Numbers in the overlapping region are shared SPMs regulated in the same direction. Numbers in parenthesis are shared SPMs regulated in the opposite direction, and are placed in the area corresponding to the direction of regulation. SPMs used for ORA analysis that are (**b**) shared and change in the same direction. Listed are all pathways and their functional categories with adjusted p-value < 0.05.

Integration analysis. We then conducted integration analysis using the joint pathway analysis module in MetaboAnalystR. By this method we found that Ras2, like Gpa2, regulated pathways related to carbohydrate, purine and certain amino acids metabolism (Tables 3 and 4, Tables S7 and S8). The extent of overlap was particularly evident through integration of the metabolomics and transcriptomics analysis. The *ras2*Δ strain was unique in regulating additional amino acids, as well as lipid and vitamin metabolism (Tables 4 and S8). The *gpa2*Δ strain was unique in regulating oxidative phosphorylation and β-alanine metabolism (Tables 3 and S7). The results obtained using MetaboAnalystR were reflected in the high confidence annotations obtained using our in-house library.

To visualize the functional relationship of Ras2 and Gpa2, we projected the inputs of our integration analysis onto the pertinent yeast metabolic pathways in KEGG. From this visualization, it is evident that the effects of Gpa2 are centered on carbohydrate and energy metabolism, which is shared by Ras2 (Figures 7a and S4). In addition, Ras2 also affects a substantial number of different metabolic species (Figures 7b and S5).

To summarize, we observed three major differences when comparing *gpr1*Δ vs. *snf3*Δ *rgt2*Δ and *gpa2*Δ vs. *ras2*Δ. First, the large and small G proteins (Gpa2 and Ras2) had concordant effects on genes and metabolites while the effects of the GPCR (Gpr1) and the transceptors (Snf3 and Rgt2) were largely opposing. Second, Ras2 had considerable effects on carbohydrate metabolism while Snf3 and Rgt2 had little effect on these processes. Third, Ras2, like Snf3 and Rgt2, affected non-carbohydrate-related pathways. However, Ras2 affected far fewer genes and metabolites, as compared to Snf3 and Rgt2. These findings highlight the functional interrelationship of the two receptor systems as well as that of the large and small G proteins.

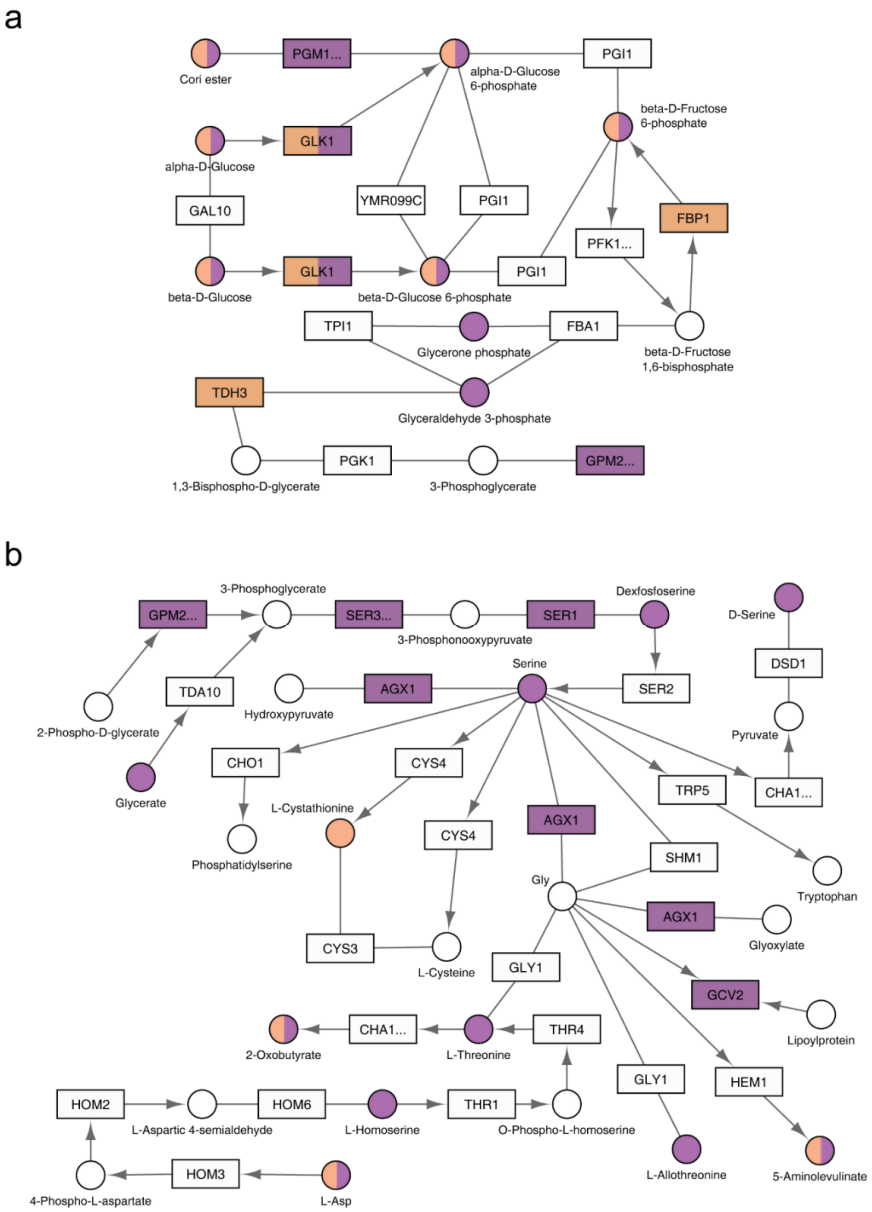

Figure 7. KEGG pathways regulated by *GPA2* or *RAS2*. The relevant part of a specific KEGG pathway is shown with genes displayed as rectangles and metabolites displayed as circles. KEGG compound name for each metabolite is labeled beside the circle. Standard gene names are labeled inside the rectangle. For enzyme complexes, the gene name for the major component is shown followed with an ellipsis. The directions of irreversible enzymatic reactions are shown by the arrows. Reversible reactions are connected by straight lines. DEGs and SPMs are highlighted in orange (*gpa2*Δ) and purple (*ras2*Δ). Shared DEGs and SPMs are colored half orange and half purple. (**a**) both *gpa2*Δ and *ras2*Δ affected components in glycolysis/gluconeogenesis (functional category: carbohydrate); (**b**) as compared with *gpa2*Δ, *ras2*Δ affected more components in glycine, serine and threonine metabolism (functional category: amino acid).

3.5. Ras2 Integrates Signals from Gpr1 and Snf3/Rgt2

Above we show that Gpr1 is dedicated to carbohydrate metabolism while Snf3 and Rgt2 primarily control the metabolism of non-carbohydrate species. The downstream G proteins, Gpa2 and Ras2, have concordant effects on carbohydrate metabolism. However, Ras2 affects additional major species that are also affected by Snf3 and Rgt2. Based on these results, we postulated that Snf3 and Rgt2 signal through Ras2. Just as Ras2 acts in synchrony

with Gpr1 and Gpa2 to regulate carbohydrate metabolism, we considered if Ras2 also works together with Snf3 and Rgt2 to regulate non-carbohydrate species. Upon examination of the integration analysis presented above, we determined that processes regulated by both Ras2 and Gpa2 are primarily related to carbohydrates (7 pathways shared), and to a lesser extent amino acids (3 pathways shared), as well as purine metabolism (Tables 3 and 4, Tables S7 and S8). In comparison, processes regulated by both Ras2 and Snf3/Rgt2 are related to amino acids (4 pathways shared), carbohydrates (4 pathways shared), peroxisome and purines (Tables 2 and 4, Tables S3 and S8).

We then quantified DEGs and SPMs regulated by Ras2 as well as by Snf3 and Rgt2. These data are presented as Venn diagrams in Figures 8a and 9a (Tables S11 and S12). In accordance with our hypothesis, ORA revealed that Ras2 and the transceptors had concordant effects on DEGs related to amino acids, energy, cofactors and vitamins (Figure 8b). While *snf3*Δ *rgt2*Δ uniquely affected some DEGs related to purines (Figure 8c), they shared with *ras2*Δ the ability to regulate SPMs related to the same process (Figure 9b). Furthermore, the effect of *ras2*Δ on carbohydrates is not shared by *snf3*Δ *rgt2*Δ (Figure 8d). We then performed qPCR to quantify the expression level of genes in wildtype, *ras2*Δ and *snf3*Δ *rgt2*Δ before and 10 min after glucose addition. As shown in Figure 10, *ras2*Δ and *snf3*Δ *rgt2*Δ have concordant effects on *INO1*, which encodes an Inositol-3-phosphate synthase, and *AGX1*, the product of which catalyzes the synthesis of glycine from glyoxylate; neither enzyme is directly related to carbohydrate metabolism. Thus, multiple lines of evidence indicate that Ras2 and the transceptors share the ability to regulate non-carbohydrate metabolism.

a

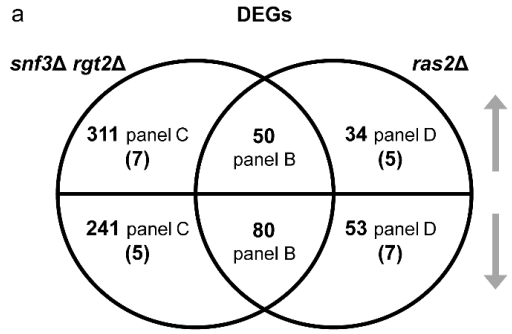

b

pathways	adjusted p-value	functional category
Nitrogen metabolism	0.0019	Energy
Biosynthesis of amino acids	0.0023	Amino acid
Glycine, serine and threonine metabolism	0.0023	Amino acid
Methane metabolism	0.0080	Energy
Carbon metabolism	0.0089	Carbohydrate
Cysteine and methionine metabolism	0.0089	Amino acid
Biosynthesis of cofactors	0.0231	Cofactors and vitamins
Vitamin B6 metabolism	0.0331	Cofactors and vitamins
Sulfur metabolism	0.0450	Energy

c

pathways	adjusted p-value	functional category
Ribosome	1.75×10^{-56}	Genetic information processing
Purine metabolism	0.0008	Nucleotide
Longevity regulating pathway	0.0020	Organismal systems

d

pathways	adjusted p-value	functional category
Starch and sucrose metabolism	5.15×10^{-8}	Carbohydrate
Carbon metabolism	2.66×10^{-5}	Carbohydrate
Galactose metabolism	0.0002	Carbohydrate
Glyoxylate and dicarboxylate metabolism	0.0003	Carbohydrate
Amino sugar and nucleotide sugar metabolism	0.0006	Carbohydrate
Pentose phosphate pathway	0.0030	Carbohydrate
Citrate cycle (TCA cycle)	0.0038	Carbohydrate
Glutathione metabolism	0.0160	Amino acid
Glycolysis / Gluconeogenesis	0.0252	Carbohydrate

Figure 8. Comparing differentially expressed genes (DEGs) of *snf3*Δ *rgt2*Δ and *ras2*Δ. (**a**) Venn diagram of subsets of DEGs, for *snf3*Δ *rgt2*Δ vs. wildtype and *ras2*Δ vs. wildtype, after glucose addition to 2%. Upper semicircle shows up-regulated DEGs and lower semicircle shows down-regulated DEGs. Numbers in the overlapping region are shared DEGs regulated in the same direction. Numbers in parenthesis are shared DEGs regulated in the opposite direction, and are placed in the area corresponding to the direction of regulation. DEGs used for ORA analysis that are (**b**) shared and change in the same direction; (**c**) unique to *snf3*Δ *rgt2*Δ; (**d**) unique to *ras2*Δ. Listed are all pathways and their functional categories with adjusted p-value < 0.05.

a

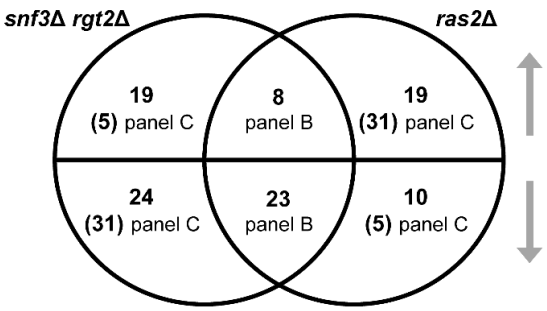

b

pathways	adjusted p-value	functional category
Purine metabolism	0.0002	Nucleotide
Alanine, aspartate and glutamate metabolism	0.0243	Amino acid

c

pathways	adjusted p-value	functional category
Amino sugar and nucleotide sugar metabolism	0.0001	Carbohydrate
Fructose and mannose metabolism	0.0003	Carbohydrate

Figure 9. Comparing significantly perturbed metabolites (SPMs) of *snf3*Δ *rgt2*Δ and *ras2*Δ. (**a**) Venn diagram of subsets of SPMs, for *snf3*Δ *rgt2*Δ vs. wildtype and *ras2*Δ vs. wildtype, after glucose addition. The upper semicircle shows up-regulated SPMs and lower semicircle shows down-regulated SPMs. Numbers in parenthesis are shared SPMs regulated in the opposite direction, and are placed in the area corresponding to the direction of regulation. Numbers in parenthesis are shared SPMs regulated in the opposite direction, and are placed in the area corresponding to the direction of regulation. SPMs used for ORA analysis that are (**b**) shared and change in the same direction; (**c**) shared and change in the opposite direction. Listed are all pathways and their functional categories with adjusted *p*-value < 0.05.

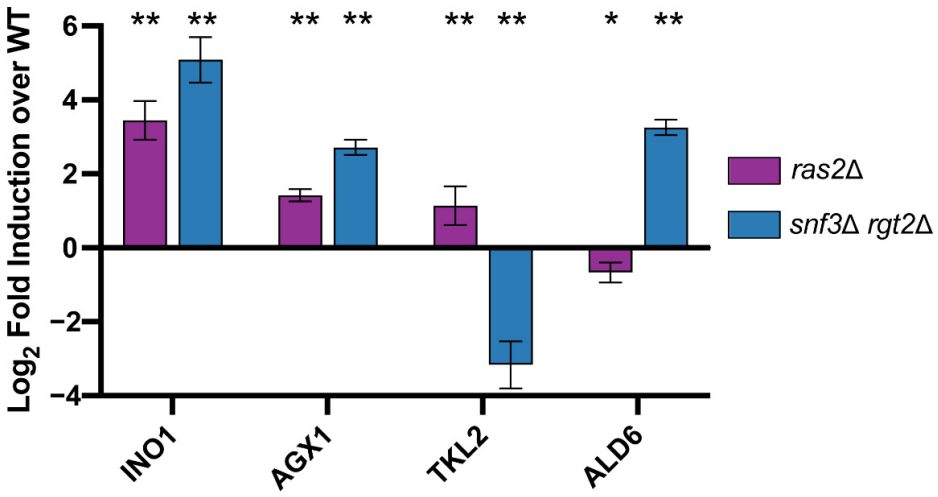

Figure 10. qPCR analysis. Bar plots of qPCR data for *INO1*, *AGX1*, *TKL2*, and *ALD6* for *ras2*Δ (purple) and *snf3*Δ *rgt2*Δ (blue). The X-axis shows target genes; Y-axis shows log2 fold induction relative to wildtype. Error bars represent standard error of mean and significance marks are as follows: $p < 0.01$(**), $p < 0.05$(*) as determined via Mann–Whitney U test and adjusted for multiple comparisons with the Benjamini–Hochberg procedure (see Methods).

As noted above, Ras2 and the transceptors had opposing effects on SPMs related to the carbohydrate metabolism (Figure 9c). This unexpected effect is further supported by qPCR analysis. As shown in Figure 10, *ras2*Δ and *snf3*Δ *rgt2*Δ had significant yet opposing impact on *TKL2*, which encodes an enzyme in the pentose phosphate pathway, and *ALD6*, which produces an aldehyde dehydrogenase involved in pyruvate metabolism. Both enzymes participate directly in carbohydrate metabolism. Therefore, the impact of Snf3 and Rgt2 on carbohydrate metabolism is more limited and antagonistic to that of Ras2. These relationships can be viewed using the KEGG Metabolic Pathways Maps (Figures S2–S5). Thus, Gpr1 and Ras2 regulate carbohydrate metabolism while Snf3/Rgt2 and Ras2 regulate non-carbohydrate metabolism. We further conclude that Ras2 coordinates and integrates signaling by both receptor systems.

4. Discussion

Integrated approaches have been used previously to compare commercially important strains of *S. cerevisiae*, by correlating production of metabolites favored in wine fermentation (e.g., ethyl and acetate esters) with differences in gene expression [80], or genomic features such as SNPs and microsatellites [81]. Correspondingly, loss of genes involved in glucose signaling influences the production of fermentation products such as glycerol, acetic acid and pyruvate [82]. Our approach has been to use integrated methods to compare signaling by key components within a common laboratory yeast strain, S288C. Most recently, we compared the function of the G-protein Gα and Gβ subunits, Gpa1 and Asc1 respectively [13]. Using global metabolomics and transcriptomics we showed that Gpa2 is primarily involved in the metabolism of sugars while Asc1 contributes to production of amino acids necessary for protein synthesis and cell division. Further, the two proteins displayed antagonistic effects on the purine metabolic pathway, mirroring their opposing effects on adenylyl cyclase activity [8,12]. In this way, we established the existence of unique and complementary functions of the two G = protein subunits.

Our present goal was to compare the function of two glucose receptors, one comprised of a G-protein coupled receptor and the other a transceptor dimer. Through a systematic analysis of individual gene deletion mutants, we showed how each system contributes—in both shared and unique ways—to transcription and metabolism. By integrating transcriptomic and metabolomic measurements, we have taken a major step by identifying new and unexpected functions of Ras2 in the transceptor signaling pathway. In addition, our integration analysis allowed us to confirm and consolidate changes seen at the metabolic or transcriptional level. Whereas the G-protein-coupled receptor directs early events in glucose utilization, the transceptors regulate subsequent processes ancillary to glucose metabolism.

While the effects of Ras2 align with those of the G-protein-coupled receptor, they also align with those of the transceptors. Based on these results, we conclude that Ras2 integrates responses from both receptor systems. Given the previous known links between Gpa2 and Ras2, we expected that mutants in those genes might have similar effects; indeed many shared effects were observed, particularly in processes related to carbohydrate metabolism. However, our global analysis suggests that a broader group of metabolic processes is affected by *ras2*Δ than by *gpa2*Δ. Further analysis is needed to understand why loss of *RAS2* has such broad impacts and what other genes are mediating that response. In the cases where *gpa2*Δ and *ras2*Δ have similar responses there may be other shared changes in activity or expression of key enzymes in the pathway. Current studies are aimed at conducting targeted metabolomics and establishing the mechanistic basis for the changes in metabolism and transcription reported here.

Less expected was the functional link between the transceptors and Ras2. Recent findings indicate that fructose-1,6-bisphosphate is an activator of the Ras proteins through the guanine nucleotide exchange factors [83]. Given that the Hxt glucose carriers have an important role in controlling glycolytic flux, and given the well-known role of Snf3 and Rgt2 in Hxt expression [47,53–62], glycolytic activation of Ras may provide an alternative link between the two glucose-sensing systems. While we do observe differences in *HXT1*, *HXT2* and *HXT5* in cells lacking *SNF3*/*RGT2* (Table S11), it should be noted that our glucose treatment was substantially shorter than that of previous studies of transcription regulation. Thus, we are likely to be missing longer term changes in hexose carrier expression. Moreover, whereas older studies relied on microarrays to quantify new gene expression, that method has largely been supplanted by RNASeq, which provides substantially greater accuracy and dynamic range of measurement. In addition, microarray data can be difficult to interpret when comparing paralogous genes since high nucleotide sequence identity can sometimes produce cross-hybridization artifacts [84,85]. Our approach is distinct from that of prior work on signaling by GPCRs and other cell surface receptors. First, protein components of cell signaling pathways have traditionally been characterized one at a time, often using different readouts for different genes or proteins. Such a piecemeal approach

has hindered a comprehensive understanding of the encoded signaling network. Our approach employed comprehensive genome-scale and metabolome-scale ("omic") measures to quantify differences between mutants lacking individual genes and gene products. Second, our approach was to compare gene deletion mutants in a single-celled organism, one where it is possible to determine functional consequences in the same genetic and epigenetic background, and under identical environmental conditions. By working with yeast, we circumvent challenges associated with more complex biological systems, where the structure or topology of the systems is not fully known, the inputs are not static but dynamic (and change over many time scales); such interactions are more likely to be nonlinear and to occur simultaneously at many levels of the biological hierarchy, from molecules to cells to tissues to organs and even to other organisms.

As part of our analysis, we compared the function of the individual transceptors, Snf3 and Rgt2, as well as two small G proteins, Ras1 and Ras2. This was done in an effort to determine how these paralogous proteins each contribute to glucose signaling, and with the expectation that such analysis could provide insights into the evolutionary forces that have preserved these gene duplications. Paralogs, or duplicated genes, are especially prevalent in processes related to glucose sensing and utilization in yeast. Apart from the transceptors and Ras proteins, at least four other components of the glucose-sensing pathway (Figure 1) and 8 (out of 12) enzymes responsible for glycolysis [86], are comprised of paralogous gene products. In comparison only 8% of chemical reactions in yeast are executed by paralogs. Systematic deletion of the glycolytic enzymes revealed no defect with respect to gene expression (by microarray), the formation of glycolytic products, or growth rate in a variety of conditions [87]. In keeping with this pattern, our transcriptomics (by RNAseq) and metabolomics analysis (by mass spectrometry) showed that Snf3 and Rgt2 are functionally redundant; that is, deletion of both genes was needed to detect any changes in the thousands of chemical entities measured here (see Data Availability Statement). Of course it is possible that differences in fitness exist but may only be evident under very specific, non-laboratory, growth conditions [86,88–91].

In the context of previous analysis of gene paralogs, we consider the most significant outcome of our analysis to be that Ras2 (but not Ras1) is required for glucose signaling, and that Ras2 is functionally linked to both receptor systems. Whereas the two receptor systems have distinct roles in signaling, Ras2 appears to integrate the two receptor pathways. Ras2, like Gpr1, directly regulates carbohydrate metabolism. Ras2, like Snf3 and Rgt2, also regulates subsequent processes related to amino acid and nitrogen metabolism. Left unresolved is the role of its paralog Ras1. One possibility is that Ras1 is primarily involved in other aspects of nutrient sensing, as demonstrated for the nitrogen-sensing pathway leading to autophagy [92].

In contrast to Ras2 and Ras1, either Snf3 or Rgt2 can sustain the glucose response. This begs the question, why have both paralogs been retained throughout the course of evolution? Most discussions of gene paralogs have focused on their potential contributions to genetic robustness and phenotypic plasticity [93]. Robustness refers to a number of different mechanisms that stabilize phenotype against genetic or environmental perturbations. An extreme example of robustness is where one of the genes is inactivated and the remaining copy provides enough of the original function to compensate for the loss and ensure survival. In support of this model, several studies in yeast have found that about a third of paralogous gene pairs exhibit negative epistasis [91,94–96], meaning that deleting both copies produces a significantly larger defect than that of the individual deletions. Robustness could be important when the activity of a duplicated gene product is temporarily disabled in response to changing environmental circumstances, for example through substrate inhibition or feedback phosphorylation. In that case the remaining paralog might compensate for the loss of its sibling by modifying its function through transcriptional reprograming [97,98], changes in protein stability and abundance [99,100], or redistribution within the cell [93,101,102]. In this way, the overall system may exhibit robustness even while the underlying components exhibit functional plasticity.

Looking forward, we plan to investigate metabolic changes over longer time periods and to use complementary approaches such as ^{13}C flux analysis. There is reason to think that such approaches will provide distinct and complementary information. In one implementation, ^{13}C flux analysis and metabolomics showed that different strains have different metabolic profiles that do not correlate with metabolic flux [103]. Rather, intracellular flux distributions fell into two different modes, one for yeast strains that exhibit respirofermentative metabolism (high glucose uptake and fermentation to ethanol) and another for those with obligate-aerobic or respiratory metabolism (low glucose uptake rates without fermentation). Recently-described methods have also used time course data from unlabeled metabolomics measurements to provide quantitative flux estimates [104]. Collectively, these approaches will aid in the interpretation of metabolomics data in highly dynamic metabolic systems.

Finally, our approach in yeast could guide investigations of functional redundancies in other signaling systems and in other organisms. For example, in humans there are three subtypes of Gαi, which assemble with four (out of five) subtypes of Gβ and 12 subtypes of Gγ. Investigators have struggled to find any functional differences among various Gβγ subunit combinations. Another example is the three isoforms of RAS in humans. These proteins were long thought to be functionally interchangeable, since all three share substantial sequence identity in domains responsible for nucleotide binding, GTPase activity, and most effector interactions. However, more recent investigations have shown that HRAS, NRAS and KRAS, when mutated, are each associated with a distinct group of cancer types [105]. An unresolved question is the physiological consequences of these differences with respect to metabolic programming. Moving forward, we believe that the comprehensive, multi-faceted approach taken here could help to provide mechanistic insights to differences among various G-proteins in humans.

Supplementary Materials: The following supporting information can be downloaded at: https://www.mdpi.com/article/10.3390/biom12020175/s1, Figure S1: PCA plots; Figure S2: Overview of DEGs and SPMs regulated by *GPR1* projected on KEGG Metabolic Pathway; Figure S3: Overview of DEGs and SPMs regulated by *SNF3* and *RGT2* projected on KEGG Metabolic Pathway; Figure S4: Overview of DEGs and SPMs regulated by *GPA2* projected on KEGG Metabolic Pathway; Figure S5: Overview of DEGs and SPMs regulated by *RAS2* projected on KEGG Metabolic Pathway; Table S1: Single-omics analysis results for wildtype between 2% (H) and 0.05% (L) glucose; Table S2: Results and statistics of transcriptomics, metabolomics and multi -omics integration for *gpr1*Δ, each as a separate sheet; Table S3: Results and statistics of transcriptomics, metabolomics and multi -omics integration for *snf3*Δ *rgt2*Δ, each as a separate sheet; Table S4: List of DEGs for each subset of the Venn diagram in Figure 2A; Table S5: List of SPMs for each subset of the Venn diagram in Figure 3A; Table S6: In-house compound identification; Table S7: Results and statistics of transcriptomics, metabolomics and multi -omics integration for *gpa2*Δ, each as a separate sheet; Table S8: Results and statistics of transcriptomics, metabolomics and multi-omics integration for *ras2*Δ, each as a separate sheet; Table S9: List of DEGs for each subset of the Venn diagram in Figure 5A; Table S10: List of SPMs for each subset of the Venn diagram in Figure 6A; Table S11: List of DEGs for each subset of the Venn diagram in Figure 8A; Table S12: List of SPMs for each subset of the Venn diagram in Figure 9A.

Author Contributions: Conceptualization, S.L., Y.L., S.E.H., D.D., S.J.S. and H.G.D.; methodology, S.L., Y.L., B.R.R., S.E.H., D.D., S.J.S. and H.G.D.; validation, S.L., Y.L., B.R.R., S.E.H., S.L.M. and D.D.; formal analysis, S.L., Y.L., B.R.R., S.E.H., S.L.M. and D.D.; investigation, S.L., Y.L., B.R.R., S.E.H., S.L.M., D.D., S.J.S. and H.G.D.; resources, S.J.S.; data curation, S.L., Y.L., B.R.R. and S.E.H.; writing—original draft preparation, S.L., S.J.S. and H.G.D.; writing—review and editing, S.L., Y.L., B.R.R., S.E.H., S.L.M., D.D., S.J.S. and H.G.D.; visualization, S.L. and S.E.H.; supervision, D.D., S.J.S. and H.G.D.; project administration, S.L., Y.L., D.D., S.J.S. and H.G.D.; funding acquisition, D.D., S.J.S. and H.G.D. All authors have read and agreed to the published version of the manuscript.

Funding: This research was funded by National Institutes of Health T32 GM008570 (S.E.H.), R35GM142864 (D.D.), R35GM118105 (H.G.D.), and institutional funding (to S.J.S., https://uncnri.org/staff-members/susan-sumner-ph-d/, accessed on 30 December 2021).

Data Availability Statement: RNA-seq data: https://www.ncbi.nlm.nih.gov/geo/query/acc.cgi?acc=GSE171846, accessed on 30 December 2021, Metabolomics data: http://dx.doi.org/10.21228/M80D82, accessed on 30 December 2021.

Acknowledgments: We thank Amy Perou and Piotr Mieczkowski at the High Throughput Sequencing Facility at UNC Chapel Hill for collecting RNAseq data. This manuscript is part of a special issue, "Transmembrane and Intracellular Signal Transduction Mechanisms", honoring Jeremy Thorner for his outstanding achievements in basic science and for the dedicated mentoring of many scientists including H.G.D.

Conflicts of Interest: The authors declare no conflict of interest.

References

1. Kresnowati, M.T.; van Winden, W.A.; Almering, M.J.; ten Pierick, A.; Ras, C.; Knijnenburg, T.A.; Daran-Lapujade, P.; Pronk, J.T.; Heijnen, J.J.; Daran, J.M. When transcriptome meets metabolome: Fast cellular responses of yeast to sudden relief of glucose limitation. *Mol. Syst. Biol.* **2006**, *2*, 49. [CrossRef] [PubMed]
2. Castrillo, J.I.; Zeef, L.A.; Hoyle, D.C.; Zhang, N.; Hayes, A.; Gardner, D.C.; Cornell, M.J.; Petty, J.; Hakes, L.; Wardleworth, L.; et al. Growth control of the eukaryote cell: A systems biology study in yeast. *J. Biol.* **2007**, *6*, 4. [CrossRef] [PubMed]
3. Gutteridge, A.; Pir, P.; Castrillo, J.I.; Charles, P.D.; Lilley, K.S.; Oliver, S.G. Nutrient control of eukaryote cell growth: A systems biology study in yeast. *BMC Biol.* **2010**, *8*, 68. [CrossRef] [PubMed]
4. Dikicioglu, D.; Karabekmez, E.; Rash, B.; Pir, P.; Kirdar, B.; Oliver, S.G. How yeast re-programmes its transcriptional profile in response to different nutrient impulses. *BMC Syst. Biol.* **2011**, *5*, 148. [CrossRef]
5. Yun, C.W.; Tamaki, H.; Nakayama, R.; Yamamoto, K.; Kumagai, H. G-protein coupled receptor from yeast Saccharomyces cerevisiae. *Biochem. Biophys. Res. Commun.* **1997**, *240*, 287–292. [CrossRef]
6. Yun, C.W.; Tamaki, H.; Nakayama, R.; Yamamoto, K.; Kumagai, H. Gpr1p, a putative G-protein coupled receptor, regulates glucose- dependent cellular cAMP level in yeast Saccharomyces cerevisiae. *Biochem. Biophys. Res. Commun.* **1998**, *252*, 29–33. [CrossRef]
7. Xue, Y.; Batlle, M.; Hirsch, J.P. GPR1 encodes a putative G protein-coupled receptor that associates with the Gpa2p Galpha subunit and functions in a Ras-independen t pathway. *EMBO J.* **1998**, *17*, 1996–2007. [CrossRef]
8. Colombo, S.; Ma, P.; Cauwenberg, L.; Winderickx, J.; Crauwels, M.; Teunissen, A.; Nauwelaers, D.; de Winde, J.H.; Gorwa, M.F.; Colavizza, D.; et al. Involvement of distinct G-proteins, Gpa2 and Ras, in glucose- and intracellular acidification-induced cAMP signalling in the yeast Saccharomyces cerevisiae. *EMBO J.* **1998**, *17*, 3326–3341. [CrossRef]
9. Kraakman, L.; Lemaire, K.; Ma, P.; Teunissen, A.W.; Donaton, M.C.; Van Dijck, P.; Winderickx, J.; de Winde, J.H.; Thevelein, J.M. A Saccharomyces cerevisiae G-protein coupled receptor, Gpr1, is specifically required for glucose activation of the cAMP pathway during the transition to growth on glucose. *Mol. Microbiol.* **1999**, *32*, 1002–1012. [CrossRef]
10. Lorenz, M.C.; Pan, X.; Harashima, T.; Cardenas, M.E.; Xue, Y.; Hirsch, J.P.; Heitman, J. The G protein-coupled receptor gpr1 is a nutrient sensor that regulates pseudohyphal differentiation in Saccharomyces cerevisiae. *Genetics* **2000**, *154*, 609–622. [CrossRef]
11. Lemaire, K.; Van de Velde, S.; Van Dijck, P.; Thevelein, J.M. Glucose and sucrose act as agonist and mannose as antagonist ligands of the G protein-coupled receptor Gpr1 in the yeast Saccharomyces cerevisiae. *Mol. Cell* **2004**, *16*, 293–299. [CrossRef]
12. Zeller, C.E.; Parnell, S.C.; Dohlman, H.G. The RACK1 ortholog Asc1 functions as a G-protein beta subunit coupled to glucose responsiveness in yeast. *J. Biol. Chem.* **2007**, *282*, 25168–25176. [CrossRef]
13. Li, S.; Li, Y.; Rushing, B.R.; Harris, S.E.; McRitchie, S.L.; Jones, J.C.; Dominguez, D.; Sumner, S.J.; Dohlman, H.G. Multi-omics analysis of glucose-mediated signaling by a moonlighting Gbeta protein Asc1/RACK1. *PLoS Genet.* **2021**, *17*, e1009640. [CrossRef]
14. Broek, D.; Toda, T.; Michaeli, T.; Levin, L.; Birchmeier, C.; Zoller, M.; Powers, S.; Wigler, M. The S. cerevisiae CDC25 gene product regulates the RAS/adenylate cyclase pathway. *Cell* **1987**, *48*, 789–799. [CrossRef]
15. Munder, T.; Kuntzel, H. Glucose-induced cAMP signaling in Saccharomyces cerevisiae is mediated by the CDC25 protein. *FEBS Lett.* **1989**, *242*, 341–345. [CrossRef]
16. Crechet, J.B.; Poullet, P.; Mistou, M.Y.; Parmeggiani, A.; Camonis, J.; Boy-Marcotte, E.; Damak, F.; Jacquet, M. Enhancement of the GDP-GTP exchange of RAS proteins by the carboxyl-terminal domain of SCD25. *Science* **1990**, *248*, 866–868. [CrossRef]
17. Jones, S.; Vignais, M.L.; Broach, J.R. The CDC25 protein of Saccharomyces cerevisiae promotes exchange of guanine nucleotides bound to ras. *Mol. Cell. Biol.* **1991**, *11*, 2641–2646.
18. Papasavvas, S.; Arkinstall, S.; Reid, J.; Payton, M. Yeast alpha-mating factor receptor and G-protein-linked adenylyl cyclase inhibition requires RAS2 and GPA2 activities. *Biochem. Biophys. Res. Commun.* **1992**, *184*, 1378–1385. [CrossRef]
19. Boy-Marcotte, E.; Ikonomi, P.; Jacquet, M. SDC25, a dispensable Ras guanine nucleotide exchange factor of Saccharomyces cerevisiae differs from CDC25 by its regulation. *Mol. Biol. Cell* **1996**, *7*, 529–539. [CrossRef]
20. Gross, A.; Winograd, S.; Marbach, I.; Levitzki, A. The N-terminal half of Cdc25 is essential for processing glucose signaling in Saccharomyces cerevisiae. *Biochemistry* **1999**, *38*, 13252–13262. [CrossRef]
21. VanderSluis, B.; Hess, D.C.; Pesyna, C.; Krumholz, E.W.; Syed, T.; Szappanos, B.; Nislow, C.; Papp, B.; Troyanskaya, O.G.; Myers, C.L.; et al. Broad metabolic sensitivity profiling of a prototrophic yeast deletion collection. *Genome Biol.* **2014**, *15*, R64. [CrossRef] [PubMed]

22. Powers, S.; Kataoka, T.; Fasano, O.; Goldfarb, M.; Strathern, J.; Broach, J.; Wigler, M. Genes in S. cerevisiae encoding proteins with domains homologous to the mammalian ras proteins. *Cell* **1984**, *36*, 607–612. [CrossRef]
23. Toda, T.; Uno, I.; Ishikawa, T.; Powers, S.; Kataoka, T.; Broek, D.; Cameron, S.; Broach, J.; Matsumoto, K.; Wigler, M. In yeast, RAS proteins are controlling elements of adenylate cyclase. *Cell* **1985**, *40*, 27–36. [CrossRef]
24. Uno, I.; Mitsuzawa, H.; Matsumoto, K.; Tanaka, K.; Oshima, T.; Ishikawa, T. Reconstitution of the GTP-dependent adenylate cyclase from products of the yeast CYR1 and RAS2 genes in Escherichia coli. *Proc. Natl. Acad. Sci. USA* **1985**, *82*, 7855–7859. [CrossRef]
25. Field, J.; Nikawa, J.; Broek, D.; MacDonald, B.; Rodgers, L.; Wilson, I.A.; Lerner, R.A.; Wigler, M. Purification of a RAS-responsive adenylyl cyclase complex from Saccharomyces cerevisiae by use of an epitope addition method. *Mol. Cell. Biol.* **1988**, *8*, 2159–2165.
26. Nakafuku, M.; Obara, T.; Kaibuchi, K.; Miyajima, I.; Miyajima, A.; Itoh, H.; Nakamura, S.; Arai, K.; Matsumoto, K.; Kaziro, Y. Isolation of a second yeast Saccharomyces cerevisiae gene (GPA2) coding for guanine nucleotide-binding regulatory protein: Studies on its structure and possible functions. *Proc. Natl. Acad. Sci. USA* **1988**, *85*, 1374–1378. [CrossRef]
27. Field, J.; Xu, H.P.; Michaeli, T.; Ballester, R.; Sass, P.; Wigler, M.; Colicelli, J. Mutations of the adenylyl cyclase gene that block RAS function in Saccharomyces cerevisiae. *Science* **1990**, *247*, 464–467. [CrossRef]
28. Suzuki, N.; Choe, H.R.; Nishida, Y.; Yamawaki-Kataoka, Y.; Ohnishi, S.; Tamaoki, T.; Kataoka, T. Leucine-rich repeats and carboxyl terminus are required for interaction of yeast adenylate cyclase with RAS proteins. *Proc. Natl. Acad. Sci. USA* **1990**, *87*, 8711–8715. [CrossRef]
29. Mintzer, K.A.; Field, J. Interactions between adenylyl cyclase, CAP and RAS from Saccharomyces cerevisiae. *Cell. Signal.* **1994**, *6*, 681–694. [CrossRef]
30. Bhattacharya, S.; Chen, L.; Broach, J.R.; Powers, S. Ras membrane targeting is essential for glucose signaling but not for viability in yeast. *Proc. Natl. Acad. Sci. USA* **1995**, *92*, 2984–2988. [CrossRef]
31. Kubler, E.; Mosch, H.U.; Rupp, S.; Lisanti, M.P. Gpa2p, a G-protein alpha-subunit, regulates growth and pseudohyphal development in Saccharomyces cerevisiae via a cAMP-dependent mechanism. *J. Biol. Chem.* **1997**, *272*, 20321–20323. [CrossRef]
32. Rolland, F.; De Winde, J.H.; Lemaire, K.; Boles, E.; Thevelein, J.M.; Winderickx, J. Glucose-induced cAMP signalling in yeast requires both a G-protein coupled receptor system for extracellular glucose detection and a separable hexose kinase-dependent sensing process. *Mol. Microbiol.* **2000**, *38*, 348–358. [CrossRef]
33. Wang, Y.; Pierce, M.; Schneper, L.; Guldal, C.G.; Zhang, X.; Tavazoie, S.; Broach, J.R. Ras and Gpa2 mediate one branch of a redundant glucose signaling pathway in yeast. *PLoS Biol.* **2004**, *2*, E128. [CrossRef]
34. Matsumoto, K.; Uno, I.; Oshima, Y.; Ishikawa, T. Isolation and characterization of yeast mutants deficient in adenylate cyclase and cAMP-dependent protein kinase. *Proc. Natl. Acad. Sci. USA* **1982**, *79*, 2355–2359. [CrossRef]
35. Kataoka, T.; Broek, D.; Wigler, M. DNA sequence and characterization of the S. cerevisiae gene encoding adenylate cyclase. *Cell* **1985**, *43*, 493–505. [CrossRef]
36. Casperson, G.F.; Walker, N.; Bourne, H.R. Isolation of the gene encoding adenylate cyclase in Saccharomyces cerevisiae. *Proc. Natl. Acad. Sci. USA* **1985**, *82*, 5060–5063. [CrossRef]
37. Harashima, T.; Heitman, J. The Galpha protein Gpa2 controls yeast differentiation by interacting with kelch repeat proteins that mimic Gbeta subunits. *Mol. Cell* **2002**, *10*, 163–173. [CrossRef]
38. Toda, T.; Cameron, S.; Sass, P.; Zoller, M.; Scott, J.D.; McMullen, B.; Hurwitz, M.; Krebs, E.G.; Wigler, M. Cloning and characterization of BCY1, a locus encoding a regulatory subunit of the cyclic AMP-dependent protein kinase in Saccharomyces cerevisiae. *Mol. Cell. Biol.* **1987**, *7*, 1371–1377.
39. Toda, T.; Cameron, S.; Sass, P.; Zoller, M.; Wigler, M. Three different genes in S. cerevisiae encode the catalytic subunits of the cAMP-dependent protein kinase. *Cell* **1987**, *50*, 277–287. [CrossRef]
40. Cannon, J.F.; Tatchell, K. Characterization of Saccharomyces cerevisiae genes encoding subunits of cyclic AMP-dependent protein kinase. *Mol. Cell. Biol.* **1987**, *7*, 2653–2663.
41. Robertson, L.S.; Fink, G.R. The three yeast A kinases have specific signaling functions in pseudohyphal growth. *Proc. Natl. Acad. Sci. USA* **1998**, *95*, 13783–13787. [CrossRef] [PubMed]
42. Pan, X.; Heitman, J. Cyclic AMP-dependent protein kinase regulates pseudohyphal differentiation in Saccharomyces cerevisiae. *Mol. Cell. Biol.* **1999**, *19*, 4874–4887. [CrossRef]
43. Robertson, L.S.; Causton, H.C.; Young, R.A.; Fink, G.R. The yeast A kinases differentially regulate iron uptake and respiratory function. *Proc. Natl. Acad. Sci. USA* **2000**, *97*, 5984–5988. [CrossRef] [PubMed]
44. Ptacek, J.; Devgan, G.; Michaud, G.; Zhu, H.; Zhu, X.; Fasolo, J.; Guo, H.; Jona, G.; Breitkreutz, A.; Sopko, R.; et al. Global analysis of protein phosphorylation in yeast. *Nature* **2005**, *438*, 679–684. [CrossRef] [PubMed]
45. Neigeborn, L.; Schwartzberg, P.; Reid, R.; Carlson, M. Null mutations in the SNF3 gene of Saccharomyces cerevisiae cause a different phenotype than do previously isolated missense mutations. *Mol. Cell. Biol.* **1986**, *6*, 3569–3574. [PubMed]
46. Ozcan, S.; Dover, J.; Rosenwald, A.G.; Wolfl, S.; Johnston, M. Two glucose transporters in Saccharomyces cerevisiae are glucose sensors that generate a signal for induction of gene expression. *Proc. Natl. Acad. Sci. USA* **1996**, *93*, 12428–12432. [CrossRef] [PubMed]
47. Ozcan, S.; Dover, J.; Johnston, M. Glucose sensing and signaling by two glucose receptors in the yeast Saccharomyces cerevisiae. *EMBO J.* **1998**, *17*, 2566–2573. [CrossRef]

48. Schmidt, M.C.; McCartney, R.R.; Zhang, X.; Tillman, T.S.; Solimeo, H.; Wolfl, S.; Almonte, C.; Watkins, S.C. Std1 and Mth1 proteins interact with the glucose sensors to control glucose-regulated gene expression in Saccharomyces cerevisiae. *Mol. Cell. Biol.* **1999**, *19*, 4561–4571. [CrossRef]
49. Lafuente, M.J.; Gancedo, C.; Jauniaux, J.C.; Gancedo, J.M. Mth1 receives the signal given by the glucose sensors Snf3 and Rgt2 in Saccharomyces cerevisiae. *Mol. Microbiol.* **2000**, *35*, 161–172. [CrossRef]
50. Spielewoy, N.; Flick, K.; Kalashnikova, T.I.; Walker, J.R.; Wittenberg, C. Regulation and recognition of SCFGrr1 targets in the glucose and amino acid signaling pathways. *Mol. Cell. Biol.* **2004**, *24*, 8994–9005. [CrossRef]
51. Moriya, H.; Johnston, M. Glucose sensing and signaling in Saccharomyces cerevisiae through the Rgt2 glucose sensor and casein kinase I. *Proc. Natl. Acad. Sci. USA* **2004**, *101*, 1572–1577. [CrossRef]
52. Pasula, S.; Jouandot, D., 2nd; Kim, J.H. Biochemical evidence for glucose-independent induction of HXT expression in Saccharomyces cerevisiae. *FEBS Lett.* **2007**, *581*, 3230–3234. [CrossRef]
53. Tomas-Cobos, L.; Sanz, P. Active Snf1 protein kinase inhibits expression of the Saccharomyces cerevisiae HXT1 glucose transporter gene. *Biochem. J.* **2002**, *368*, 657–663. [CrossRef]
54. Kim, J.H.; Polish, J.; Johnston, M. Specificity and regulation of DNA binding by the yeast glucose transporter gene repressor Rgt1. *Mol. Cell. Biol.* **2003**, *23*, 5208–5216. [CrossRef]
55. Flick, K.M.; Spielewoy, N.; Kalashnikova, T.I.; Guaderrama, M.; Zhu, Q.; Chang, H.C.; Wittenberg, C. Grr1-dependent inactivation of Mth1 mediates glucose-induced dissociation of Rgt1 from HXT gene promoters. *Mol. Biol. Cell* **2003**, *14*, 3230–3241. [CrossRef]
56. Mosley, A.L.; Lakshmanan, J.; Aryal, B.K.; Ozcan, S. Glucose-mediated phosphorylation converts the transcription factor Rgt1 from a repressor to an activator. *J. Biol. Chem.* **2003**, *278*, 10322–10327. [CrossRef]
57. Lakshmanan, J.; Mosley, A.L.; Ozcan, S. Repression of transcription by Rgt1 in the absence of glucose requires Std1 and Mth1. *Curr. Genet.* **2003**, *44*, 19–25. [CrossRef]
58. Polish, J.A.; Kim, J.H.; Johnston, M. How the Rgt1 transcription factor of Saccharomyces cerevisiae is regulated by glucose. *Genetics* **2005**, *169*, 583–594. [CrossRef]
59. Kim, J.H.; Johnston, M. Two glucose-sensing pathways converge on Rgt1 to regulate expression of glucose transporter genes in Saccharomyces cerevisiae. *J. Biol. Chem.* **2006**, *281*, 26144–26149. [CrossRef]
60. Palomino, A.; Herrero, P.; Moreno, F. Tpk3 and Snf1 protein kinases regulate Rgt1 association with Saccharomyces cerevisiae HXK2 promoter. *Nucleic Acids Res.* **2006**, *34*, 1427–1438. [CrossRef]
61. Jouandot, D., 2nd; Roy, A.; Kim, J.H. Functional dissection of the glucose signaling pathways that regulate the yeast glucose transporter gene (HXT) repressor Rgt1. *J. Cell. Biochem.* **2011**, *112*, 3268–3275. [CrossRef] [PubMed]
62. Roy, A.; Shin, Y.J.; Cho, K.H.; Kim, J.H. Mth1 regulates the interaction between the Rgt1 repressor and the Ssn6-Tup1 corepressor complex by modulating PKA-dependent phosphorylation of Rgt1. *Mol. Biol. Cell* **2013**, *24*, 1493–1503. [CrossRef] [PubMed]
63. Brachmann, C.B.; Davies, A.; Cost, G.J.; Caputo, E.; Li, J.; Hieter, P.; Boeke, J.D. Designer deletion strains derived from Saccharomyces cerevisiae S288C: A useful set of strains and plasmids for PCR-mediated gene disruption and other applications. *Yeast* **1998**, *14*, 115–132. [CrossRef]
64. Dobin, A.; Davis, C.A.; Schlesinger, F.; Drenkow, J.; Zaleski, C.; Jha, S.; Batut, P.; Chaisson, M.; Gingeras, T.R. STAR: Ultrafast universal RNA-seq aligner. *Bioinformatics* **2013**, *29*, 15–21. [CrossRef]
65. Patro, R.; Duggal, G.; Love, M.I.; Irizarry, R.A.; Kingsford, C. Salmon provides fast and bias-aware quantification of transcript expression. *Nat. Methods* **2017**, *14*, 417–419. [CrossRef]
66. Love, M.I.; Huber, W.; Anders, S. Moderated estimation of fold change and dispersion for RNA-seq data with DESeq2. *Genome Biol.* **2014**, *15*, 550. [CrossRef]
67. Love, M.I.; Anders, S.; Kim, V.; Huber, W. RNA-Seq workflow: Gene-level exploratory analysis and differential expression. *F1000Research* **2015**, *4*, 1070. [CrossRef]
68. Yu, G.; Wang, L.G.; Han, Y.; He, Q.Y. clusterProfiler: An R package for comparing biological themes among gene clusters. *OMICS* **2012**, *16*, 284–287. [CrossRef]
69. Li, Y.Y.; Douillet, C.; Huang, M.; Beck, R.; Sumner, S.J.; Styblo, M. Exposure to inorganic arsenic and its methylated metabolites alters metabolomics profiles in INS-1 832/13 insulinoma cells and isolated pancreatic islets. *Arch. Toxicol.* **2020**, *94*, 1955–1972. [CrossRef]
70. Zelena, E.; Dunn, W.B.; Broadhurst, D.; Francis-McIntyre, S.; Carroll, K.M.; Begley, P.; O'Hagan, S.; Knowles, J.D.; Halsall, A.; Consortium, H.; et al. Development of a robust and repeatable UPLC-MS method for the long-term metabolomic study of human serum. *Anal. Chem.* **2009**, *81*, 1357–1364. [CrossRef]
71. Dunn, W.B.; Broadhurst, D.; Begley, P.; Zelena, E.; Francis-McIntyre, S.; Anderson, N.; Brown, M.; Knowles, J.D.; Halsall, A.; Haselden, J.N.; et al. Procedures for large-scale metabolic profiling of serum and plasma using gas chromatography and liquid chromatography coupled to mass spectrometry. *Nat. Protoc.* **2011**, *6*, 1060–1083. [CrossRef]
72. Chong, J.; Wishart, D.S.; Xia, J. Using MetaboAnalyst 4.0 for Comprehensive and Integrative Metabolomics Data Analysis. *Curr. Protoc. Bioinform.* **2019**, *68*, e86. [CrossRef]
73. Pang, Z.; Chong, J.; Li, S.; Xia, J. MetaboAnalystR 3.0: Toward an Optimized Workflow for Global Metabolomics. *Metabolites* **2020**, *10*, 186. [CrossRef]
74. Kanehisa, M.; Goto, S. KEGG: Kyoto encyclopedia of genes and genomes. *Nucleic Acids Res.* **2000**, *28*, 27–30. [CrossRef]
75. Kanehisa, M. Toward understanding the origin and evolution of cellular organisms. *Protein Sci.* **2019**, *28*, 1947–1951. [CrossRef]

76. Kanehisa, M.; Furumichi, M.; Sato, Y.; Ishiguro-Watanabe, M.; Tanabe, M. KEGG: Integrating viruses and cellular organisms. *Nucleic Acids Res.* **2020**. [CrossRef]
77. Zhang, N.; Cao, L. Starvation signals in yeast are integrated to coordinate metabolic reprogramming and stress response to ensure longevity. *Curr. Genet.* **2017**, *63*, 839–843. [CrossRef]
78. Li, S.; Park, Y.; Duraisingham, S.; Strobel, F.H.; Khan, N.; Soltow, Q.A.; Jones, D.P.; Pulendran, B. Predicting network activity from high throughput metabolomics. *PLoS Comput. Biol.* **2013**, *9*, e1003123. [CrossRef]
79. Colombo, S.; Ronchetti, D.; Thevelein, J.M.; Winderickx, J.; Martegani, E. Activation state of the Ras2 protein and glucose-induced signaling in Saccharomyces cerevisiae. *J. Biol. Chem.* **2004**, *279*, 46715–46722. [CrossRef]
80. Mendes, I.; Sanchez, I.; Franco-Duarte, R.; Camarasa, C.; Schuller, D.; Dequin, S.; Sousa, M.J. Integrating transcriptomics and metabolomics for the analysis of the aroma profiles of Saccharomyces cerevisiae strains from diverse origins. *BMC Genom.* **2017**, *18*, 455. [CrossRef]
81. Franco-Duarte, R.; Umek, L.; Mendes, I.; Castro, C.C.; Fonseca, N.; Martins, R.; Silva-Ferreira, A.C.; Sampaio, P.; Pais, C.; Schuller, D. New integrative computational approaches unveil the Saccharomyces cerevisiae pheno-metabolomic fermentative profile and allow strain selection for winemaking. *Food Chem.* **2016**, *211*, 509–520. [CrossRef]
82. Vallejo, B.; Peltier, E.; Garrigos, V.; Matallana, E.; Marullo, P.; Aranda, A. Role of Saccharomyces cerevisiae Nutrient Signaling Pathways During Winemaking: A Phenomics Approach. *Front. Bioeng. Biotechnol.* **2020**, *8*, 853. [CrossRef]
83. Peeters, K.; Van Leemputte, F.; Fischer, B.; Bonini, B.M.; Quezada, H.; Tsytlonok, M.; Haesen, D.; Vanthienen, W.; Bernardes, N.; Gonzalez-Blas, C.B.; et al. Fructose-1,6-bisphosphate couples glycolytic flux to activation of Ras. *Nat. Commun.* **2017**, *8*, 922. [CrossRef] [PubMed]
84. Xing, Y.; Stoilov, P.; Kapur, K.; Han, A.; Jiang, H.; Shen, S.; Black, D.L.; Wong, W.H. MADS: A new and improved method for analysis of differential alternative splicing by exon-tiling microarrays. *RNA* **2008**, *14*, 1470–1479. [CrossRef] [PubMed]
85. Kapur, K.; Jiang, H.; Xing, Y.; Wong, W.H. Cross-hybridization modeling on Affymetrix exon arrays. *Bioinformatics* **2008**, *24*, 2887–2893. [CrossRef] [PubMed]
86. Bradley, P.H.; Gibney, P.A.; Botstein, D.; Troyanskaya, O.G.; Rabinowitz, J.D. Minor Isozymes Tailor Yeast Metabolism to Carbon Availability. *Msystems* **2019**, *4*, e00170-18. [CrossRef]
87. Solis-Escalante, D.; Kuijpers, N.G.; Barrajon-Simancas, N.; van den Broek, M.; Pronk, J.T.; Daran, J.M.; Daran-Lapujade, P. A Minimal Set of Glycolytic Genes Reveals Strong Redundancies in Saccharomyces cerevisiae Central Metabolism. *Eukaryot. Cell* **2015**, *14*, 804–816. [CrossRef]
88. Giaever, G.; Chu, A.M.; Ni, L.; Connelly, C.; Riles, L.; Veronneau, S.; Dow, S.; Lucau-Danila, A.; Anderson, K.; Andre, B.; et al. Functional profiling of the Saccharomyces cerevisiae genome. *Nature* **2002**, *418*, 387–391. [CrossRef]
89. Papp, B.; Pal, C.; Hurst, L.D. Metabolic network analysis of the causes and evolution of enzyme dispensability in yeast. *Nature* **2004**, *429*, 661–664. [CrossRef]
90. Ihmels, J.; Collins, S.R.; Schuldiner, M.; Krogan, N.J.; Weissman, J.S. Backup without redundancy: Genetic interactions reveal the cost of duplicate gene loss. *Mol. Syst. Biol.* **2007**, *3*, 86. [CrossRef]
91. DeLuna, A.; Vetsigian, K.; Shoresh, N.; Hegreness, M.; Colon-Gonzalez, M.; Chao, S.; Kishony, R. Exposing the fitness contribution of duplicated genes. *Nat. Genet.* **2008**, *40*, 676–681. [CrossRef]
92. Jin, X.; Starke, S.; Li, Y.; Sethupathi, S.; Kung, G.; Dodhiawala, P.; Wang, Y. Nitrogen Starvation-induced Phosphorylation of Ras1 Protein and Its Potential Role in Nutrient Signaling and Stress Response. *J. Biol. Chem.* **2016**, *291*, 16231–16239. [CrossRef]
93. Nijhout, H.F.; Sadre-Marandi, F.; Best, J.; Reed, M.C. Systems Biology of Phenotypic Robustness and Plasticity. *Integr. Comp. Biol.* **2017**, *57*, 171–184. [CrossRef]
94. Dean, E.J.; Davis, J.C.; Davis, R.W.; Petrov, D.A. Pervasive and persistent redundancy among duplicated genes in yeast. *PLoS Genet.* **2008**, *4*, e1000113. [CrossRef]
95. Musso, G.; Costanzo, M.; Huangfu, M.; Smith, A.M.; Paw, J.; San Luis, B.J.; Boone, C.; Giaever, G.; Nislow, C.; Emili, A.; et al. The extensive and condition-dependent nature of epistasis among whole-genome duplicates in yeast. *Genome Res.* **2008**, *18*, 1092–1099. [CrossRef]
96. VanderSluis, B.; Bellay, J.; Musso, G.; Costanzo, M.; Papp, B.; Vizeacoumar, F.J.; Baryshnikova, A.; Andrews, B.; Boone, C.; Myers, C.L. Genetic interactions reveal the evolutionary trajectories of duplicate genes. *Mol. Syst. Biol.* **2010**, *6*, 429. [CrossRef]
97. Gu, X.; Zhang, Z.; Huang, W. Rapid evolution of expression and regulatory divergences after yeast gene duplication. *Proc. Natl. Acad. Sci. USA* **2005**, *102*, 707–712. [CrossRef]
98. Kafri, R.; Bar-Even, A.; Pilpel, Y. Transcription control reprogramming in genetic backup circuits. *Nat. Genet.* **2005**, *37*, 295–299. [CrossRef]
99. DeLuna, A.; Springer, M.; Kirschner, M.W.; Kishony, R. Need-based up-regulation of protein levels in response to deletion of their duplicate genes. *PLoS Biol.* **2010**, *8*, e1000347. [CrossRef]
100. Van der Lee, R.; Lang, B.; Kruse, K.; Gsponer, J.; Sanchez de Groot, N.; Huynen, M.A.; Matouschek, A.; Fuxreiter, M.; Babu, M.M. Intrinsically disordered segments affect protein half-life in the cell and during evolution. *Cell Rep.* **2014**, *8*, 1832–1844. [CrossRef]
101. Stelling, J.; Sauer, U.; Szallasi, Z.; Doyle, F.J., 3rd; Doyle, J. Robustness of cellular functions. *Cell* **2004**, *118*, 675–685. [CrossRef] [PubMed]

102. Kitano, H. Biological robustness. *Nat. Rev. Genet.* **2004**, *5*, 826–837. [CrossRef] [PubMed]
103. Christen, S.; Sauer, U. Intracellular characterization of aerobic glucose metabolism in seven yeast species by 13C flux analysis and metabolomics. *FEMS Yeast Res.* **2011**, *11*, 263–272. [CrossRef] [PubMed]
104. Bordbar, A.; Yurkovich, J.T.; Paglia, G.; Rolfsson, O.; Sigurjonsson, O.E.; Palsson, B.O. Elucidating dynamic metabolic physiology through network integration of quantitative time-course metabolomics. *Sci. Rep.* **2017**, *7*, 46249. [CrossRef]
105. Zhou, B.; Der, C.J.; Cox, A.D. The role of wild type RAS isoforms in cancer. *Semin. Cell Dev. Biol.* **2016**, *58*, 60–69. [CrossRef]